



## Key drivers of pyrogenic carbon redistribution during a simulated rainfall event

Severin-Luca Bellè<sup>1</sup>, Asmeret Asefaw Berhe<sup>2</sup>, Frank Hagedorn<sup>3</sup>, Cristina Santin<sup>4,5</sup>, Marcus Schiedung<sup>1</sup>, Ilja van Meerveld<sup>1</sup> and Samuel Abiven<sup>1,6</sup>

- 5 <sup>1</sup>Department of Geography, University of Zurich, Switzerland  
<sup>2</sup>Department of Life and Environmental Sciences, University of California, Merced, CA, USA  
<sup>3</sup>Swiss Federal Institute for Forest, Snow and Landscape Research WSL, Switzerland  
<sup>4</sup>Department of Biosciences, College of Science, Swansea University, Swansea, UK  
<sup>5</sup>Unidad Mixta de Investigación en Biodiversidad, Oviedo University, Mieres, Spain  
10 <sup>6</sup>Laboratoire de Géologie, Département de Géosciences, École Normale Supérieure, Paris, France

Correspondence to: Samuel Abiven (abiven@biotite.ens.fr)

**Abstract.** Pyrogenic carbon (PyC) is produced by the incomplete combustion of vegetation during wildfires and is a major and persistent pool of the global carbon (C) cycle. However, its redistribution in the landscape after fires remains largely unknown. Therefore, we conducted rainfall simulation experiments on 0.25-m<sup>2</sup> plots with two distinct Swiss forest soils  
15 (Cambisol (clay loam) and Luvisol (sandy silt)). We applied PyC produced from wood (*Picea abies*) labelled under FACE conditions and C4-grass (*Miscanthus sinensis*) to the soil surface to study PyC redistribution by runoff and splash, and the vertical mobility of PyC in a 10 cm unsaturated soil column based on the differences in  $\delta^{13}\text{C}$  of soils and PyC. We assessed the effect of soil texture, slope angle and PyC characteristics (feedstock and particle size) on the mobility of PyC during 30  
20 minutes of intense rainfall (102 mm h<sup>-1</sup>). Our results highlight that PyC is highly mobile. Surface runoff transported between 0.2 to 36.0 % of the total added PyC. Erosion by splash further redistributed 10.3 to 25.3 % of the added PyC. Soil type had a substantial impact on the redistribution of PyC by both runoff and splash: on average, we recovered 10.5 % of the added PyC in runoff and splashed material for the clay-rich Cambisol and 61.3 % of the added PyC for the sandy silt Luvisol combined. PyC feedstock had a clear, but contrasting effect on PyC redistribution: relocation in the runoff and splashed material was  
25 greater for wood-PyC (43.4 % of total added PyC) than grass-PyC (28.4 %). However, more wood-PyC (11.5 %; fraction of organic C derived from the PyC) remained where it was initially applied compared to grass-PyC (7.4 %). The results further suggest that the effect of PyC characteristics on its mobility can be highly variable and depend not only on the material from which it was derived, but also on other factors (e.g. particle size, porosity, density). In particular, the mobility of PyC was almost twice as large for fine-grained PyC (< 63  $\mu\text{m}$ ) than for coarse PyC (63  $\mu\text{m}$  – 2 mm). Vertical mobility of PyC up to  
30 to 10 cm depth was greater in the clay-rich, well-aggregated Cambisol, but limited in the physically instable Luvisol, likely due to quick aggregate breakdown and surface sealing. The addition of PyC to the surface of the studied soils further induced changes in the export of native soil organic carbon (nSOC) in the same order of magnitude as the PyC flux after the 30 minutes rainfall event. Our study shows that large quantities of PyC can be redistributed by water erosion over short timescales, and



that the mobility of PyC depends to a great extent on the response of soils to rainfall. Moreover, the addition and redistribution of PyC affects the export of nSOC, and thus the C budget of fire-affected soils and catchments.

## 35 1 Introduction

Wildfires burn 345 to 464 Mha, i.e. 4 % of the vegetated land area, annually and are thus a major disturbance for terrestrial ecosystems (Giglio et al., 2013; Randerson et al., 2012). The associated carbon (C) flux of 2.2 Pg to the atmosphere affects the global C cycle and the Earth's climate (Bowman et al., 2009; van der Werf et al., 2017). It is predicted that fire frequencies will increase in many regions around the world due to climate change. This amplifies the importance of fires for key  
40 biogeochemical and climate processes and its correct representation in earth system models (Conard and Solomon, 2009; Lasslop et al., 2019; Westerling et al., 2006). In addition to the impact on atmospheric C emissions, wildfires also affect the global C cycle through the impact on the earth's surface processes (Lasslop et al., 2019). The incomplete combustion of  
45 vegetation during fires produces a continuum of C-rich materials with polycyclic, condensed aromatic molecular structures, ranging from soot to macroscopic charcoal (Bird et al., 2015; Hammes and Abiven, 2013). The global production of this fire-derived or pyrogenic C (PyC) is estimated to be 192 to 340 Tg PyC annually (Jones et al., 2019; Santín et al., 2016). PyC is  
50 environmentally more resistant than its unburnt precursors and can remain in terrestrial and aquatic ecosystems for decades to millennia (Abiven and Santín, 2019; Coppola and Druffel, 2016; Santín et al., 2016). It is one of the largest and oldest C pools on Earth (Bird et al., 2015) and globally accounts for around 15 % of organic carbon (OC) in soils (Reisser et al., 2016). However, we currently have little knowledge about the fate of PyC in the landscape and the dominant processes that lead to  
55 its mobilization, degradation, and stabilization at different landscape positions and at the interface between land and ocean still need to be clarified (Abiven and Santín, 2019; Abney and Berhe, 2018; Masiello and Berhe, 2020).

Erosion by water represents a fundamental transport process for soil organic carbon (SOC) and PyC in terrestrial, sloping landscapes and determines its export to aquatic systems (Abney and Berhe, 2018; Berhe et al., 2018). Water erosion refers here to the detachment of particles by raindrop impact, subsequent transport by water, and final deposition (Berhe et al., 2018;  
55 Doetterl et al., 2016). It takes place as splash erosion, interrill erosion, and rill/gully erosion (de Nijs and Cammeraat, 2020). Erosion globally causes the redistribution of 10 to 140 Pg of soil  $y^{-1}$  (Berhe et al., 2018; Doetterl et al., 2016). Estimates of global SOC erosion range between 0.3 to 5 Pg  $y^{-1}$  (Berhe et al., 2007; Chappell et al., 2016; Lal, 2004; Stallard, 1998); and for PyC it has been estimated to be between 3 to 5 Tg  $y^{-1}$  based on field investigations in Mediterranean climate (Abney et al.,  
60 2017) and 29 to 87 Tg  $y^{-1}$  based on modelling of global PyC dynamics (Bird et al., 2015). The diverse methods used to quantify PyC contributes to the large variability in reported values of PyC erosion. Physical (based on size and density of PyC), chemical (based on the oxidation resistance of PyC), thermal (based on temperature resistance of PyC), spectroscopic (based on magnetic or photonic response of PyC to input signal) and molecular marker (based on identification of PyC specific compounds) methods cover different windows of the PyC continuum and, therefore, estimates of PyC movement in the landscape can vary substantially (Bird et al., 2015; Hammes and Abiven, 2013).



65 Erosion by water can have a profound impact on the persistence and fate of SOC and PyC as it can transfer these forms of OC  
from eroding landscapes to depositional sites where they can be preserved for a long time (Abney et al., 2017; Abney and  
Berhe, 2018). However, it can also accelerate decomposition of SOC and PyC by physical disintegration (Abney et al., 2019a;  
Pignatello et al., 2015) and biochemical degradation during and after transport (Hilscher and Knicker, 2011; Singh et al., 2012).  
Although it was debated in the past if erosion by water is a net C sink or source (Doetterl et al., 2016), it is nowadays considered  
70 to be a C sink. However, the size of the erosion-induced C sink still needs to be assessed (Abney and Berhe, 2018; Berhe et  
al., 2018).

In post-fire landscapes erosion by water is very often substantially enhanced (Abney and Berhe, 2018; Masiello and Berhe,  
2020; Vieira et al., 2018). The removal of the protective vegetation cover during wildfires increases the impact of raindrops  
on the soil surface (Certini, 2005; Johansen et al., 2001; Pierson et al., 2013), which can cause aggregate breakdown and  
75 surface sealing (Moody et al., 2013; Shakesby, 2011). The effects of fire-induced changes on the structural and hydrological  
properties of soils and erosion depend on the fire regime (frequency, severity, intensity, and extent), precipitation pattern  
(timing, frequency, intensity, watershed hydrology), vegetation (fuel load, ground cover, regrowth dynamics), topography  
(slope steepness, aspect, and length, micro-topography) and soil properties (texture, aggregation, saturation) (Abney and Berhe,  
2018; Archibald et al., 2013; Berhe et al., 2012; Moody et al., 2013; Rumpel et al., 2015; Shakesby and Doerr, 2006). Soil  
80 type determines the extent to which erodible materials are susceptible to detachment and mobilization and, together with the  
local geomorphology, governs soil physical stability and therefore erodibility (Moody et al., 2013; Vieira et al., 2015).

The PyC particles produced during a fire that remain on the soil surface may be more redistributed by water erosion during the  
first rainfall than other soil particles (Abney et al., 2019b; Rumpel et al., 2009, 2006). This high mobilization of PyC is partially  
caused by its physical properties, in particular its low density and high porosity, but also due to the lack of organo-mineral  
85 interactions between the PyC and soil matrix that prevent either wash-out (surface erosion by interrill or splash) or wash-in (to  
deeper soil horizons) during initial rainfall (Brewer et al., 2014; Masiello and Berhe, 2020; Pyle et al., 2017). Most PyC  
materials have a high initial hydrophobicity, which can promote floating and transport by water (Abney and Berhe, 2018;  
Rumpel et al., 2015). The transport of PyC also depends on the material from which it was derived, with grass-derived PyC  
being perceived to be more mobile than wood-PyC (Saiz et al., 2018). Here, the physical stability of PyC plays a role: PyC  
90 that can be fragmented more easily will produce smaller particles (Pignatello et al., 2015; Saiz et al., 2018) that are more  
mobile (Masiello, 2004; Saiz et al., 2018; Santín et al., 2016). This fragmentation depends on the transformation of cell  
structures during pyrolysis and it is usually higher for grass than for wood materials (Chrzazvez et al., 2014).

The combined effects of climate, vegetation, fire, catchment topography and hydrology, soils and PyC properties will result in  
spatially variable post-fire redistribution of PyC (Abney and Berhe, 2018; Berhe et al., 2018; Moody et al., 2013). However,  
95 to which extent these drivers affect the magnitude of post-fire PyC erosion and deposition still need to be elucidated (Abney  
and Berhe, 2018; Berhe et al., 2018; Santín et al., 2016). It is difficult to assess the redistribution of PyC directly after a fire  
because substantial redistribution occurs during the first major rainfall event (Masiello and Berhe, 2020). Rainfall simulation  
experiments allow controllability and comparability between drivers, so that a diverse set of drivers can be repeatedly studied



100 from a mechanistic point of view under the same conditions (Doetterl et al., 2016; Rumpel et al., 2015). Furthermore, it is crucial to study individual transport processes of PyC in closed systems where PyC redistribution can be assessed fully with a single, direct tracer method that allows for sufficient replication under the same controlled conditions.

The objectives of this study were to assess the initial redistribution of PyC during major rainfall events on soils through splash and runoff, as well as its vertical movement in the soil column, and how this depends on soil texture, slope angle, and PyC characteristics (feedstock and particle size). Therefore, we conducted a simulated rainfall experiment on 0.25-m<sup>2</sup> soil plots on which wood- and grass-PyC with a different isotopic signal ( $\delta^{13}\text{C}$ ) than the soils was applied. We estimated PyC redistribution by collecting it in the runoff sediment, splashed sediment, floating particles, as well as soil cores and by measuring the relative contribution of PyC to the  $\delta^{13}\text{C}$  signal of the sediments, floating particles and soil cores. Specifically, we determined: (a) the effect of soil texture, slope angle and PyC characteristics on the transport of PyC by surface runoff (i.e., overland flow), (b) the effect of soil texture, slope angle and PyC characteristics on PyC redistribution by splash, (c) the effect of soil texture, slope angle and PyC characteristics on the wash-in of PyC into the soil and (d) the effect of the application of PyC on the redistribution of native soil organic carbon (nSOC).

## 2 Material and methods

### 2.1 General approach

We used rainfall simulation experiments to study PyC erosion and transport on soil plots. We used two forest soils with different properties (Sect. 2.2 and Table 1) that had been unburnt for at least 20 years and added wood- or grass-PyC (Sect. 2.3 and Table 2) to the surface of the uppermost third of the 0.25-m<sup>2</sup> plot. We used a multi-factorial experimental design that included two elements of four key drivers of PyC relocation based on literature evidence. These included soil texture (clayey loam (Cambisol) vs. sandy silt (Luvisol)), slope angle (10 ° vs. 25 °), PyC feedstock (wood-PyC vs. grass-PyC) and PyC particle size (< 63  $\mu\text{m}$  vs. 63  $\mu\text{m}$  - 2 mm). Each of the two elements of the four drivers were combined and assessed in triplicates (48 plots). In addition, for soil texture and slope we also used four replicate control plots (16 plots) where no PyC was added (hereafter labelled as “CT”). During each experimental run, rainfall was applied for 30 minutes to one control plot and three plots where PyC was added. These were randomly selected (total 16 runs). The applied rainfall had an intensity of 102.8 mm h<sup>-1</sup> (51.4  $\pm$  1.4 mm of applied rainfall in total). After the rainfall simulation ended, we collected the sediment that was transported by the runoff and the sediment that was splashed to the sides and, also, took soil cores to determine the redistribution of PyC across the plots and the vertical transport of PyC in the soil. We used the  $\delta^{13}\text{C}$  signal of the added PyC materials as a direct tracer of PyC in this study to overcome methodological limitations of other PyC detection methods.

### 2.2 Soils

We used the top 20 cm (without vegetation and litter) of two Swiss forest soils that differ in soil texture, soil stability, SOC content, and soil hydrological properties (Table 1). The first soil is a Cambisol (IUSS Working Group WRB, 2015), collected



130 from the Laegern site, next to the CarboEurope forest flux site (CH-LAE, 47°28'42.0" N; 8°21'51.8" E), which is a site of  
the Long-term Forest Ecosystem Research (LWF) of the Swiss Federal Institute for Forest, Snow and Landscape Research  
(WSL). The site is located at 700 m a.s.l. on the Laegern mountain, which belongs to the Swiss Jura and is a mixed mountain  
forest dominated by beech, ash, fir, lime and spruce (Ruehr et al., 2010). It has a clayey loam texture, high aggregate stability  
(mean weight diameter (MWD) =  $1.74 \pm 0.03$ ), and SOC content of  $3.6 \pm 0.4$  % (Table 1). The second soil is a haplic Luvisol  
135 that was collected from the Moehlin site (Intercantonal Forest Observation Program in Switzerland). The Moehlin site is  
located on an alluvial deposit close to the river Rhine (47°35'06.0" N; 7°52'34.3" E) at an elevation of 290 m a.s.l, and is  
dominated by a woodruff beech forest stand (Braun et al., 2020). The soil has a sandy silt texture, medium aggregate stability  
(MWD =  $0.89 \pm 0.03$ ) and an SOC content of  $2.24 \pm 0.02$  % (Table 1). In the following, the soils are named as "Cambisol"  
and "Luvisol", respectively. The collected soils were kept indoor under a protective foil and regularly rewetted with deionized  
140 water prior to the experiments. The soils were not sieved to  $< 2$  mm due to the considerable amount of soil material  
(approximately 1 ton of each soil). Even though a soil that had been burned on the surface would have been more realistic, we  
used unburnt soils for practical reasons (large volume of soils, homogeneity of the surface, reproducibility of fire conditions,  
control of initial PyC amount).

### 2.3 Pyrogenic carbon (PyC) material: production and characterization

145 We used two types of PyC material (Table 2): PyC from spruce wood (*Picea abies*, hereafter called wood-PyC and labelled  
with "W") grown under FACE conditions (Free Air Carbon Dioxide Enrichment; Hagedorn et al., 2003) and PyC from  
*Miscanthus* grass (*Miscanthus sinensis*), a C4-plant (Hilber et al., 2012) (hereafter called grass-PyC and labelled with "G").  
The PyC was produced in several batches through pyrolysis, following the established method described in Hammes et al.  
(2006). Briefly, the biomass was loaded in a quartz tube (small chips of wood and grass of several centimetres in size), heated  
150 to 450 °C in a pyrolysis oven and charred for 4 h under a continuous N<sub>2</sub> stream, and collected after cooling. Pyrolysis has little  
effect on the  $\delta^{13}\text{C}$  of PyC ( $-38.0 \pm 0.2$  ‰ for spruce wood vs  $-38.2 \pm 0.2$  ‰ for wood-PyC; and  $-12.7 \pm 0.1$  ‰ for *Miscanthus*  
grass vs  $-13.8 \pm 0.1$  ‰ for grass-PyC). Mean mass recovery was  $31.0 \pm 0.5$  %, which is in line with yields reported by Keiluweit  
et al. (2010) for both grass- and wood PyC at comparable charring temperatures (400 to 500 °C). Afterwards, we homogenized  
the PyC of all batches by careful mixing them in a bowl. To produce two sizes of PyC particles, we first passed the PyC through  
155 a 2 mm sieve and retained it on a 63  $\mu\text{m}$  sieve to obtain the coarse particles (63  $\mu\text{m}$  – 2 mm, hereafter labelled with "CP").  
Afterwards, a subsample was milled and passed through the 63  $\mu\text{m}$  sieve (hereafter labelled with "FP"). Each of the two PyC  
particle size fractions was homogenized by mixing and aliquots were sampled for characterization.  
We determined PyC water repellency using the Ethanol droplet test, as described in Doerr (1998). The wood- and grass-PyC  
were both extremely hydrophobic, with no detectable differences between them (Table 2). We characterised the PyC material  
160 by diffuse reflectance infrared Fourier-transformed spectroscopy (DRIFT) analysis (TENSOR 27 spectrophotometer, Bruker  
Fällanden, Switzerland). DRIFT spectra highlighted a higher aromaticity and condensation for the wood-PyC, as indicated  
through higher absorption at 1730-1680  $\text{cm}^{-1}$  assigned to carbonyl/carboxyl C=O and at 1610-1570  $\text{cm}^{-1}$  assigned to aromatic



C=C (Fig. S1). Cell structures were also better preserved for the wood-PyC than the grass-PyC, as indicated by a higher absorption for cellulose (C-O) at 1260-1210  $\text{cm}^{-1}$  (Chatterjee et al., 2012; Keiluweit et al., 2010).

## 165 2.4 Plot preparation

For the experiments, we used a soil plot (0.5 x 0.5 x 0.2 m; 0.25- $\text{m}^2$  flume) and added clean Styrofoam (so that water can still drain) to the bottom 10 cm. We added the soil on top of the Styrofoam to reach a soil thickness of 10-12 cm and slightly compressed it to avoid any bagging of soil during experiments (bulk density between 0.9 (Cambisol) and 1.0  $\text{g}/\text{cm}^3$  (Luvisol)). We took particular care to also fill the edges of the plots and levelled the surface with a metal bar. We then applied the PyC

170 material evenly on the surface of the uppermost third of the plot (upslope). The application rate was 118.7  $\text{g PyC m}^{-2}$  (equal of 77.0  $\pm$  1.5  $\text{g C}$  for wood-PyC (Total C = 64.9  $\pm$  1.3 %) and 81.4  $\pm$  2.1  $\text{g C}$  for grass-PyC (Total C = 68.6  $\pm$  1.8 %)) and we let it settle for at least one hour to simulate surface deposition (Fig. 1). We choose this application rate based on literature estimates of standing biomass per  $\text{m}^2$  and PyC production and post-fire deposition (Proulx et al., 2015; Santín et al., 2015), and application rates (106  $\text{g m}^{-2}$ ) used in field plot studies on PyC erosion (Rumpel et al., 2009).

175 The surface of the prepared plots were photographed with a high-end Sony Alpha 7R III & Zeiss Batis 18 mm fixed wide-angle lens (4K resolution with Pixel Shift Technology) attached to a tripod (fixed distance and angle to the floor) (Fig. 1b). Prior to rainfall simulation, the plots were adjusted to the respective slope angle (10 ° or 25 °) and an overflow (metal plate) was added to the lowest sidewall and connected to a runoff channel and bucket (Fig. 1a). We monitored soil moisture in each plot with a Decagon Em50 (inserted at 5 cm depth). Finally, we installed the splash shelter (corrugated panel) around each plot

180 to ensure a closed system (Fig. 1a).

## 2.5 Rainfall simulation

We used the indoor, gravity-type rainfall simulator at the Swiss Federal Institute for Forest, Snow and Landscape Research (WSL) for the rainfall simulation experiments. The simulator includes drop-producing needles with an inner diameter of 0.05 mm and a drop fall height of 7 to 8.5 m. The setup and general principles of the simulator have been described in detail

185 in Berger et al. (2010) and basic data (i.e., water pressure, flow, temperature, rainfall characteristics) can be found in the Supporting Material (Table S1 and Fig. S2). The simulator setup produced raindrops that reached terminal velocities and drop size distribution (determined using the oil method (Kathiravelu et al., 2016); data not shown) close to natural rainfalls (Abd Elbasit et al., 2010; Abudi et al., 2012; Aksoy et al., 2012). We used only one simulator element (1.05 x 3.25 m) and a designated area of 0.8 x 2.8 m under the simulator for the experiments. This allowed us to place four of the 0.25- $\text{m}^2$  plots side

190 by side below the simulator and apply rainfall to them simultaneously. The rainfall intensity in the simulation area was measured three times using 56 small (8.5 cm diameter) funnel gauges (Fig. S2). The simulator produced constant rainfall of 102.8  $\text{mm h}^{-1}$  (51.4  $\pm$  1.4 mm in 30 minutes). The Christiansen uniformity coefficient of 84 % indicates a uniform distribution of the rainfall over the simulation area (Aksoy et al., 2012; Christiansen, 1942; Lassu and Seeger, 2015).



195 Because we applied rainfall to four plots at a time, we prioritised homogeneous distribution of rainfall over the simulated area  
to ensure controlled and comparable conditions between the plots. The uniformity of the rainfall over the simulation area  
decreased rapidly with intensities smaller than  $100 \text{ mm h}^{-1}$ , and therefore this intensity was chosen. The simulated rainfall  
depth of 51.4 mm for 30 minutes represents a rainfall event with a return interval of 51-206 years for three long term  
meteorological stations near the Laegern site (Zurich Kloten: 206 (95 % confidence interval: 51 to > 300), Zurich Affoltern:  
69 (21 to > 300) and Zurich Fluntern: 93 (25.5 to > 300)). For the stations in close proximity to the Moehlin site it represents  
200 an event with a return interval of 99-117 years (Rünenberg: 98.5 (25 to > 300) and Basel: 116.5 (28 to > 300); 1982-2018 data  
(Federal Office of Meteorology and Climatology MeteoSwiss, 2019)).

## 2.6 Sampling, sample preparation and analysis

After the rainfall simulation experiment, we flushed the runoff channel with a known volume of deionized water and recorded  
the total weight of the bucket that already contained the surface runoff and the eroded material. To collect splash sediment, we  
205 washed the splash panel with a known volume of deionized water and collected it in the splash basin that already contained  
the eroded splash material. We transferred all the collected splash material to a bucket and weighed it. The buckets with the  
runoff and splashed material were set aside for sedimentation for > 24 hours before carefully collecting the particles floating  
on the water surface, pumping out the water with a bell jar attached to a peristaltic pump and finally collecting the sediment  
that settled at the bottom of the buckets. The sediment and floating particles of both the runoff and the splashed material were  
210 separately dried at  $40 \text{ }^{\circ}\text{C}$  and weighed. Finally, sediment samples of both the runoff and splash were milled. The floating  
particles of both the runoff and splash were milled in a mortar by hand because of the small amount of material. The collected  
sediment and floating particles were analysed for total organic carbon (TOC; representing nSOC for control plots and nSOC  
+ PyC for plots where PyC was applied) and  $\delta^{13}\text{C}$ , relative to the international Vienna Pee Dee Belemnite (VPDB) standard,  
using cavity ring-down spectroscopy with a dry combustion system (CRDS Picarro, Inc. 2020).  
215 Prior to sampling the soil after the experiment, each plot was photographed as described previously (i.e., similar as before the  
rainfall simulation). We sampled the soil with a soil corer (steel cylinder with a 5 cm diameter and 10 cm length). We took  
cores at three random locations in the three slope positions (upslope, midslope, downslope), cut the cores into three depth  
increments (0-1, 1-3 and 3-10 cm) and homogenized the material from the three cores per depth to obtain one composite sample  
per slope position, depth and plot. Soil samples were air-dried, sieved to < 2 mm and milled. The soil samples were analysed  
220 similarly as the collected sediment and floating particles for TOC and  $\delta^{13}\text{C}$ . Additionally, we took cores from control plots for  
each soil before and after rainfall simulation and analysed them for the bulk density. We also tested the aggregate stability  
(mean weight diameter (MWD) calculation) of the soils with the fast wetting method described in Le Bissonnais (2016). Using  
the same method as for PyC materials, we tested soil water repellence according to the Ethanol droplet test of Doerr (1998).



## 2.7 Quantification of the PyC contribution to TOC using $\delta^{13}\text{C}$ and C recovery

225 To determine PyC redistribution during a rainfall event, we used the differences in  $\delta^{13}\text{C}$  of the forest soils ( $-29.1 \pm 0.1 \text{ ‰}$  for  
the Cambisol and  $-29.9 \pm 0.1 \text{ ‰}$  for the Luvisol) and the PyC materials ( $-38.2 \pm 0.2 \text{ ‰}$  for the wood-PyC and  $-13.8 \pm 0.1 \text{ ‰}$   
for the grass-PyC). The  $\delta^{13}\text{C}$  difference of 8.3 to 16.1 ‰ between the soils and PyC materials was much larger than the maximal  
drift of the CRDS analyser ( $< 0.5 \text{ ‰}$ ) and allowed us to differentiate between nSOC and PyC in the TOC. We used a two-pool  
isotope-mixing model to calculate the contribution of the added PyC to the  $\delta^{13}\text{C}$ -signal of a sample (sediment, floating particles  
230 or soil cores) using Eq. (1):

$$f = 1 - \left( \frac{(\delta^{13}\text{C}_{\text{sample}} - \delta^{13}\text{C}_{\text{PyC\_app}})}{(\delta^{13}\text{C}_{\text{control}} - \delta^{13}\text{C}_{\text{PyC\_app}})} \right) \times 100 \quad (1)$$

where  $f$  is the fraction of OC derived from the PyC (or PyC fraction, in %),  $\delta^{13}\text{C}_{\text{sample}}$  is the  $\delta^{13}\text{C}$  value of the sample,  $\delta^{13}\text{C}_{\text{PyC\_app}}$   
is the average  $\delta^{13}\text{C}$  value of the added PyC (Table 2), and  $\delta^{13}\text{C}_{\text{control}}$  is the average  $\delta^{13}\text{C}$  value of the control plots for the runoff,  
splashed sediments, runoff and splash floating particles respectively (representing the nSOC of the TOC). The PyC fraction  
235 (in %) was subsequently multiplied with the TOC (nSOC + PyC, in g) and finally the quantity of PyC (in g C) was divided by  
the amount of added PyC (in g C) to calculate PyC recovery (% of total added PyC). For the soil core calculations (Fig. 6 and  
Table S2), we used the average  $\delta^{13}\text{C}$  value of all control samples (Table 1) to ensure a stable background signal to calculate  
the PyC fraction. For the soil core samples, we could not convert the PyC fraction to a reliable PyC recovery value, because  
both the soil mass and the TOC contents of the soil core samples were too variable.

## 240 2.8 Statistical analyses

We ran Levene's test to check the homogeneity of variance assumption (center = mean). We ran a two-way ANOVA model  
for the full dataset on eroded soil mass, eroded TOC, PyC recovery (runoff and splash sediment, runoff and splash floating  
particles), and subsequently a two-way ANOVA model per soil type (Cambisol and Luvisol) for the same datasets. For the  
soil core data, we used a two-way ANOVA model for each slope position (upslope, midslope and downslope) and depth  
245 increment (0-1, 1-3, 3-10 cm) for the full dataset and subsequently for the individual soil types. We used the Shapiro-Wilk  
tests on the ANOVA residuals to check the normality assumption and Fisher's least significant difference (LSD) post-hoc tests  
( $\alpha = 0.05$ ,  $p_{\text{adj}} = \text{bonferroni}$ ) on the two elements of the four drivers. For changes in nSOC export after application of  
PyC compared to corresponding controls, we used a Welch two sample t-test (95 % confidence interval). All statistical analyses  
were completed using the R packages "agricolae" and "car" in RStudio Version 3.5.2 (R Core Team, 2018).



## 250 3 Results

### 3.1 Redistribution of soil and total organic carbon (TOC)

#### 3.1.1 Amount of runoff and relocated quantities of soil and floating particles

The amount of surface runoff generated was much less for the Cambisol than the Luvisol plots, with average runoff ratios for all plots of  $13.2 \pm 0.8 \%$  and  $88.5 \pm 2.3 \%$  respectively (Table 1). Soil moisture was higher in the Cambisol, and for both soils  
255 for the  $10^\circ$  plots than the  $25^\circ$  plots (Fig. S3). For the Cambisol, initial soil moisture increased rapidly over the first 5 minutes and then steadily increased until the end of the rainfall simulation for both slope angles. For the Luvisol, soil moisture increased rapidly, but less pronounced during the first 10 minutes and remained stable after 15 minutes for the  $10^\circ$  slope plots and after around 20 minutes for the  $25^\circ$  plots. The relatively low moisture contents of both soils at the end of the experiment and the flattening of the moisture curves towards the end of the simulation indicate that the soils were not fully saturated and infiltration  
260 rates dropped due to surface sealing, especially for the Luvisol (Fig. S3). This was also visually observed during experiments. The amount of soil that was transported by the runoff (i.e., the soil mass for control plots and soil + PyC mass for plots where PyC was applied) was significantly different for the two soil types: on average  $1.3 \pm 0.2 \text{ g}$  ( $= 5.2 \pm 0.8 \text{ g m}^{-2}$ ) for the Cambisol and  $196.7 \pm 14.3 \text{ g}$  ( $= 786.8 \pm 57.2 \text{ g m}^{-2}$ ) for the Luvisol ( $p < 0.001$ ; Fig. 2a). Note that because PyC represented  $< 2 \%$  of total mass, its influence on the total mass of transported soil could be neglected for this calculation. The runoff driven erosion rates  
265 varied between  $2.8 \pm 0.3 \text{ g m}^{-2}$  (Cambisol under  $10^\circ$  slope) to  $1156.8 \pm 160.8 \text{ g m}^{-2}$  (Luvisol under  $25^\circ$  slope) for the 30 minutes rainfall simulation. The sediment transport was about two times higher for plots under steeper slopes (average for all  $10^\circ$  plots:  $70.4 \pm 13.6 \text{ g}$  and all  $25^\circ$  plots:  $127.6 \pm 24.2 \text{ g}$ ). The effect of slope was significant for the Cambisol ( $p = 0.03$ ) and Luvisol ( $p < 0.001$ ).

Soil type was also the main explanatory variable for the average amount of soil eroded by splash (Fig. 2b). It was on average  
270 1.5 times less ( $p < 0.001$ ) for the Cambisol ( $65.5 \pm 3.6 \text{ g}$  ( $= 262.0 \pm 14.4 \text{ g m}^{-2}$ )) than the Luvisol ( $95.5 \pm 4.5 \text{ g}$  ( $= 382.0 \pm 18.0 \text{ g m}^{-2}$ )). Transport rates by splash ranged between  $178.8 \pm 16.0 \text{ g m}^{-2}$  (Cambisol under  $10^\circ$  slope) to  $468.4 \pm 73.6 \text{ g m}^{-2}$  (Luvisol under  $25^\circ$  slope) for the 30 minutes rainfall simulation.

The total transport of floating particles (i.e., native SOC (nSOC) for control plots and nSOC + PyC for plots where PyC was applied) by runoff were different between soil types. It was  $0.03 \pm 0.01 \text{ g}$  for the Cambisol and  $0.49 \pm 0.09 \text{ g}$  for the Luvisol  
275 ( $p < 0.001$ ). For PyC particle sizes, it was  $0.6 \pm 0.1 \text{ g}$  when PyC was applied as coarse particles (CP),  $0.09 \pm 0.02 \text{ g}$  for fine particles (FP) and  $0.08 \pm 0.02 \text{ g}$  for controls (CT, no PyC applied) ( $p < 0.001$ ; Fig. 2c). The mass of floating particles eroded by splash was larger than for the runoff and also dependent on soil type (Cambisol:  $0.17 \pm 0.05 \text{ g}$  and Luvisol:  $1.0 \pm 0.2 \text{ g}$ ,  $p < 0.001$ ). It further also dependent on PyC particle size (CP:  $1.4 \pm 0.3 \text{ g}$ , FP:  $0.14 \pm 0.02 \text{ g}$  and CT:  $0.10 \pm 0.02 \text{ g}$ ,  $p < 0.001$ ; Fig. 2d). However, the total mass of floating particles transported by runoff or splash was only significantly higher with the  
280 application of coarse PyC to the Luvisol (significant interaction of the drivers “Soil type x PyC particle size” in the ANOVA model:  $p < 0.001$ ).



### 3.1.2 Transported TOC

Similar to the mass of soil that was transported, the amount of TOC transported by runoff (i.e., native SOC (nSOC) for control plots and nSOC + PyC for plots where PyC was added) was almost negligible for the Cambisol, but notable for the Luvisol  
285 (0.08 ± 0.01 g C and 7.3 ± 0.5 g C respectively,  $p < 0.001$ , Fig. 3a). Steeper slope angles (25 °) resulted in 1.5 times more TOC transport by the runoff, but did not change the proportions of eroded TOC/soil. This effect holds true for both soil types (Cambisol ( $p = 0.03$ ) and Luvisol ( $p = 0.0005$ )). The strong interaction of soil type and slope in our model suggests that more TOC was transported by runoff on steeper slopes on the Luvisol in absolute terms ( $p = 0.0003$ ; Fig. 3a). Transport rates of TOC by runoff ranged between 0.08 ± 0.04 g C m<sup>2</sup> (Cambisol under 10 ° slope) to 44.0 ± 5.6 g C m<sup>2</sup> (Luvisol under 25 ° slope)  
290 for the 30 minutes rainfall simulation. We found higher export of TOC (nSOC + PyC) by runoff when fine PyC particles (FP) were applied, but not when coarse PyC particles (CP) were applied, compared to control plots (CT). However, we identified this only for the Luvisol (FP: 9.1 ± 0.8 g C, CP: 6.5 ± 0.5 g C and CT (no PyC applied): 5.8 ± 0.7 g C;  $p = 0.0009$ ), indicating that fine PyC particles preferentially contributed to the transported TOC by runoff on the Luvisol (soil type x PyC particle size:  $p = 0.003$ ; Fig. 3a).

295 Splash erosion of TOC was slightly higher for the Luvisol (Cambisol: 2.9 ± 0.2 g C and Luvisol 3.3 ± 0.2 g C,  $p = 0.05$ ; Fig. 3b). All plots of both soils receiving PyC showed higher splash erosion of TOC irrespective of PyC feedstock or particle size compared to control plots, but we found no difference between either wood- and grass-PyC or fine and coarse PyC for any of the soils (Fig. 3b). Transport rates of TOC through splash ranged between 6.8 ± 0.8 g C m<sup>2</sup> (Cambisol under 10 ° slope) to 16.4 ± 2.8 g C m<sup>2</sup> (Luvisol under 25 ° slope) for the 30 minutes rainfall simulation.

300 The transported quantities of TOC (i.e., nSOC for control plots and nSOC + PyC for plots where PyC was applied) in the floating particles for both the runoff and splash differed between the soil types and PyC particle sizes (Fig. 3c-d). The mass of relocated TOC by runoff of floating particles was 0.011 ± 0.002 g C for the Cambisol and 0.24 ± 0.04 g C for the Luvisol ( $p < 0.001$ ; Fig. 3c). Application of both wood- and grass-PyC as coarse particles resulted in more transport of TOC in floating particles by runoff compared to the control plots, but this was not the case for the fine PyC particles. The particle size was  
305 significant for the Luvisol, but not the Cambisol, which suggests that the coarse PyC contributed to the transported TOC of floating particles in the runoff for the Luvisol (soil type x PyC particle size:  $p < 0.001$ ; Fig. 3c). The mass of TOC in floating particles relocated by splash erosion was 0.06 ± 0.01 g C for the Cambisol and 0.6 ± 0.1 g C for the Luvisol ( $p < 0.001$ ; Fig. 3d). For both soils, application of wood- and grass-PyC as coarse particles resulted in more relocation of TOC in floating particles by splash compared to the controls, and again this was not the case for the fine PyC particles ( $p < 0.001$ ; Fig. 3d).

### 310 3.2 Redistribution of PyC by runoff and splash: Recovery of added PyC

We observed similar trends for the redistribution of the added PyC as for the transported soil and TOC (Fig. 2-3), including clear differences between the two soil types. PyC relocation (as % of total added PyC) through runoff and splash erosion combined, for both sediment and floating particles, varied between 10.5 ± 1.4 % for the Cambisol to 61.3 ± 3.4 % for the



Luvisol ( $p < 0.001$ ; Fig. 4). Moreover, we recovered much more of the added PyC in the sediments and floating particles  
315 transported by runoff and splash combined after application of wood- than grass- PyC (W:  $43.4 \pm 6.6$  % and G:  $28.4 \pm 4.6$  %,  $p < 0.001$ ; Fig. 4).

PyC in the runoff sediment (% of total added PyC) was more than 300 times less for the Cambisol ( $0.09 \pm 0.02$  %) than the  
Luvisol ( $32.4 \pm 3.8$  %,  $p < 0.001$ ; Fig. 4a). Application of wood-PyC resulted in more PyC relocation in sediment by runoff  
( $19.4 \pm 5.0$  %) compared to grass-PyC ( $13.1 \pm 3.3$  %), and this effect was significant for both soils (Cambisol:  $p = 0.04$  and  
320 Luvisol:  $p = 0.009$ ). Application of fine PyC ( $23.1 \pm 5.3$  %) resulted in more PyC redistribution of the sediment by runoff  
compared to coarse PyC particles ( $9.4 \pm 2.2$  %) in the full ANOVA model, but the effect differed for the two soils (Fig. 4a).  
There was more PyC relocation for coarse particles for the Cambisol ( $p = 0.01$ ; less than  $< 0.13 \pm 0.03$  % for both particle  
sizes), but, for the Luvisol, there was more PyC relocation for the fine particles (FP:  $46.1 \pm 4.6$  % and CP:  $18.7 \pm 2.0$  %,  $p <$   
 $0.001$ ). In contrast to the amount of transported soil and TOC by the runoff (Fig. 2a and 3a), slope angle did not affect PyC  
325 redistribution ( $p = 0.09$ ; Fig. 4a).

In accordance with the larger mass of splashed soil (Fig. 2b), we found greater PyC relocation (% of total added PyC) by splash  
for the Luvisol ( $15.2 \pm 1.4$  %) than the Cambisol ( $9.5 \pm 1.5$  %,  $p = 0.0006$ ; Fig. 4b). When averaged for the two soils,  
redistribution of PyC by splash was twice as much when wood-PyC ( $16.0 \pm 1.7$  %) was applied compared to grass-PyC ( $8.6 \pm$   
 $1.0$  %,  $p < 0.001$ ). Relocation of PyC by splash was greater when fine PyC particles were applied compared to coarser ones  
330 (FP:  $14.3 \pm 1.6$  % and CP:  $10.3 \pm 1.5$  %), but this effect was only significant for the Cambisol (soil type x PyC particle size:  $p$   
 $< 0.0003$ ; Fig. 4b).

Redistributed quantities of PyC as floating particles were significantly different for the two soil types and PyC particle sizes  
(Fig. 4c-d). Relocated PyC in floating particles in the runoff was  $0.07 \pm 0.03$  % of initially added PyC for the Cambisol and  
 $3.6 \pm 0.8$  % for the Luvisol ( $p < 0.001$ ; Fig. 4c). Application of coarse PyC particles resulted in significantly higher relocation  
335 of PyC in floating particles in runoff compared to finer PyC (CP:  $3.6 \pm 0.8$  % and FP:  $0.02 \pm 0.01$  %; Cambisol ( $p = 0.001$ )  
and Luvisol ( $p < 0.001$ ); Fig. 4c). Relocated PyC in floating particles of splash accounted for  $0.8 \pm 0.2$  % (Cambisol) and  $10.1$   
 $\pm 2.3$  % (Luvisol) of the recovered PyC ( $p < 0.001$ ; Fig. 4d). The amount of relocated PyC in floating particles by splash was  
higher for coarser particles than finer ones (CP:  $10.9 \pm 2.2$  % and FP:  $0.03 \pm 0.01$  %), and this effect was significant for the  
Cambisol ( $p = 0.0003$ ) and Luvisol ( $p < 0.001$ ; Fig. 4d).

### 340 3.3 Changes of nSOC dynamics after application of PyC

Our  $\delta^{13}\text{C}$  approach (using  $^{13}\text{C}$ -labelled PyC material) and the mass balance of TOC and PyC allowed us to estimate the effect  
of PyC application on the transport of native SOC (nSOC). We compared the transport of nSOC for control plots (nSOC =  
TOC) with plots where we added PyC (nSOC = TOC – PyC). Changes in nSOC export through runoff after application of PyC  
were negligible for the Cambisol ( $< 0.5 \pm 0.1$  g C  $\text{m}^2$ ), but important for the Luvisol (Fig. 5a). For the Luvisol, the changes  
345 varied from reduced export in the order of  $8.4 \pm 5.2$  g C  $\text{m}^2$  (fine-grained wood-PyC on  $25^\circ$  slope;  $p = 0.25$ ) to higher export



in the order of  $8.4 \pm 4.0$  g C m<sup>2</sup> (fine-grained grass-PyC on 10 ° slope;  $p = 0.16$ ) compared to controls (Fig. 5a). Changes of nSOC export through splash after application of PyC were important for the Cambisol at the 10 ° slope, but small for the Luvisol (Fig. 5b). For the 10 ° Cambisol plots, we observed a higher export of nSOC after PyC application than for the control plots in the range of  $3.6 \pm 1.6$  g C m<sup>2</sup> (fine-grained grass-PyC;  $p = 0.13$ ) to  $5.2 \pm 0.4$  g C m<sup>2</sup> (fine-grained wood-PyC). For the wood-PyC application, higher exports were significant for fine ( $p = 0.01$ ) and coarse PyC particles ( $p = 0.002$ ). Changes in nSOC export as floating particles through runoff and splash after PyC application were small and highly variable (Fig. 5c-d).

### 3.4 Distribution of PyC on the soil surface and in the soil

#### 3.4.1 Upslope position

For the upslope position (i.e., uppermost third where PyC was initially added), the distribution of PyC on the soil surface and in the soil after the rainfall simulation differed strongly for the two soil types (here reported as the fraction of OC derived from the PyC in % (or PyC fraction)). We found more PyC at all three depths (0-1, 1-3 and 3-10 cm) in the Cambisol than the Luvisol (Fig. 6a-b and Table S2). For the surface layer (0-1 cm), the PyC fraction was  $11.4 \pm 1.6$  % for the Cambisol and  $7.5 \pm 0.9$  % for the Luvisol ( $p = 0.0009$ ). At 1-3 cm depth, it was  $4.8 \pm 0.5$  % for the Cambisol and  $0.5 \pm 0.2$  % for the Luvisol ( $p < 0.001$ ) and at 3-10 cm depth, the difference was  $2.0 \pm 0.3$  % for the Cambisol and  $0.8 \pm 0.2$  % for the Luvisol ( $p = 0.007$ ). The visual assessment of the soil surface and vertical profile confirmed that more PyC remained on the surface or was washed in for the Cambisol than the Luvisol (Fig. 1b).

In addition to soil type, the distribution of PyC on the soil surface (0-1 cm) of the upper slope depended on PyC feedstock (Fig. 6a-b and Table S2). A larger PyC fraction remained on the surface when wood-PyC ( $11.5 \pm 1.5$  %) was applied than when grass-PyC ( $7.4 \pm 1.0$  %) was applied, and this effect was significant for the Cambisol ( $p = 0.005$ ) and Luvisol ( $p = 0.03$ ). Furthermore, significantly more PyC remained on the surface of the Cambisol when coarser PyC particles ( $18.1 \pm 1.5$  %) were applied than finer ones ( $4.6 \pm 0.7$  %;  $p < 0.001$ ). The strong interaction of soil type and PyC particle size in our model suggests that coarse PyC remained on the soil surface of the Cambisol in the upslope position ( $p < 0.001$ ; Fig. 6a and Table S2).

#### 3.4.2 Mid- and downslope

In the midslope position, significant differences were only found for the Luvisol and were mainly related to PyC feedstock (Fig. 6c-d and Table S2). There was more PyC fraction on the surface (0-1 cm) of the Luvisol when wood-PyC ( $5.0 \pm 0.9$  %) was applied than for grass-PyC ( $1.6 \pm 0.3$  %;  $p = 0.002$ ). This was also the case at 1-3 cm depth ( $1.2 \pm 0.5$  % for wood-PyC compared to  $0.3 \pm 0.2$  % for grass-PyC;  $p = 0.02$ ). In addition, there was significantly more PyC at 1-3 cm depth in the midslope position for the Cambisol than the Luvisol (PyC fraction:  $1.9 \pm 0.4$  % for the Cambisol and  $0.7 \pm 0.3$  % for the Luvisol;  $p = 0.002$ ). This difference was also seen for the downslope cores (Cambisol:  $1.9 \pm 0.5$  % and Luvisol:  $0.9 \pm 0.3$  %), but was not significant ( $p = 0.11$ ). The PyC fraction on the soil surface (0-1 cm) at the mid- and downslope positions was higher for the



Luvisol than the Cambisol (Fig. 6c-f and Fig. 1b):  $2.3 \pm 0.5$  % for the Cambisol and  $3.3 \pm 0.6$  % for the Luvisol at the midslope position ( $p = 0.14$ ). Downslope, it was  $1.1 \pm 0.4$  % for the Cambisol and  $2.3 \pm 0.5$  % for the Luvisol ( $p = 0.058$ ).

## 4 Discussion

### 4.1 PyC redistribution by rainfall

380 Our study provides evidence for a quick redistribution of PyC by intense rainfall. Between  $0.18 \pm 0.05$  % to  $36.0 \pm 4.6$  % of  
the initially added PyC was transported by runoff (both as sediment and floating particles) and between  $10.3 \pm 1.7$  % to  $25.3$   
 $\pm 3.7$  % of the initially added PyC was transported as splash (both as sediment and floating particles) during 30 minutes rainfall  
events (51.4 mm) on 0.25-m<sup>2</sup> plots (Fig. 4). Therefore, our data confirms that the fate and mobility of PyC on short timescales  
depends to a great extent on its initial interaction with water (Masiello and Berhe, 2020). The portions of PyC relocated by  
runoff (% of total added PyC; Fig. 4a and 4c) are in the same order of magnitude as observed for post-fire, plot-scale erosion  
385 field studies. Rumpel et al. (2009) reported that between 7 to 29 % of initially applied PyC was transported by runoff. Cotrufo  
et al. (2016) found that 11 % of PyC present in the organic layer was exported during the first year after a fire and Major et al.  
(2010) estimated that around 20 to 53 % of applied PyC must be relocated by erosion. In addition, Rumpel et al. (2009) reported  
PyC erosion by splash of  $31.2 \pm 21.3$  %, and our values of PyC recovery are well in this range (Fig. 4b and 4d). However, it  
390 has to be mentioned that other studies have also reported limited transport of PyC ( $< 2$  % of TOC in runoff) after 62 years after  
a fire (Güereña et al., 2015).

Initial rainfall not only determines the redistribution of PyC on the surface, but also the quantity of PyC that moves into the  
soil (Masiello and Berhe, 2020). We recovered part of the initially added PyC (PyC fraction) at 1-3 and 3-10 cm depth at the  
upslope position where it was initially applied, especially for the Cambisol (6.8 % (Cambisol) and 1.3 % (Luvisol); Fig. 6a-  
395 b). This shows that PyC moved through the soil profile within 30 minutes under unsaturated conditions. Due to the small  
amounts of PyC compared to the total mass of soil in our plots (on average  $26.0 \pm 0.2$  kg soil per plot), we could only calculate  
the fraction of OC that is PyC (PyC fraction) in the soil column, but no PyC recovery (% of total added PyC). This limits the  
comparison with literature values. We chose larger quantities of soil (larger plot size) to eliminate possible boundary effects  
of the plots on PyC redistribution. However, in accordance with our findings, vertical movement of <sup>13</sup>C-labelled wood-PyC  
400 (3-4 % of applied PyC) up to 10-15 cm depth in soil cylinders after 10 months under field conditions has been reported for one  
of the sites from which we took the soil for our plots (Cambisol at Laegern site) (Singh et al., 2014). In other studies conducted  
on soil plots or soil microcosms (between 8 to 20 cm long and 10 cm in diameter) in the field or in the laboratory, relocated  
quantities by vertical movement up to 10 cm depth after 1-2 years varied between  $< 1$  % to 2.3 % of initially applied PyC (in  
particulate or dissolved form) (Hilscher and Knicker, 2011; Maestrini et al., 2014; Major et al., 2010). Even larger amounts  
405 (23-46 % of initially applied PyC) have been reported for plot-scale rainfall simulations in the tropics, but this vertical transport  
was limited to 1 cm depth (Rumpel et al., 2009).



## 4.2 Effect of PyC application on nSOC redistribution

By using  $\delta^{13}\text{C}$ -labelled PyC, we were able to show for the first time (to our knowledge) that the application of PyC to the soil surface and its subsequent redistribution affects the fate and redistribution of native SOC (nSOC). The changes in nSOC export  
410 by runoff and splash after application of PyC were highly variable, but in the same order of magnitude as the PyC flux after the rainfall event (Fig. 5). Therefore, nSOC and PyC dynamics are linked, but the underlying processes are not fully clear. Changes in nSOC export through runoff, especially for the Luvisol, ranged from a reduced export of  $-8.4 \pm 5.2 \text{ g C m}^{-2}$  to an additional export of  $+8.4 \pm 4.0 \text{ g C m}^{-2}$  compared to nSOC export for the controls. This could be related to the sorption and stabilization of nSOC to PyC surfaces (Jiang et al., 2019; Singh et al., 2014). Since the PyC is either transported by the runoff  
415 or retained, the associated nSOC will also be redistributed or retained. Additional exports of nSOC between  $3.6 \pm 1.6 \text{ g C m}^{-2}$  to  $5.2 \pm 0.4 \text{ g C m}^{-2}$  by splash, especially for the Cambisol under  $10^\circ$  slope, can again be explained by the high affinity of nSOC to PyC surfaces and its subsequent relocation. Additional export of nSOC in the presence of PyC can further be explained by the strong affinity of PyC to sorb to mineral surfaces, which can promote the mobilization of less effectively adsorbed nSOC through desorption (Jiang et al., 2016). However, it seems unlikely that this adsorption takes place within minutes. Another  
420 explanation could be that PyC particles on the soil surface increase the soil hydrophobicity and lead to a longer contact time between water and nSOC, which may promote its export.

## 4.3 Key drivers of soil, TOC and PyC redistribution

### 4.3.1 Soil type

Soil type was the main explanatory variable that influenced soil, TOC and PyC redistribution by surface runoff (Fig. 2a, 3a  
425 and 4a). This can be related to the soils' physical and hydrological properties. The higher runoff (7 times higher for the Luvisol than the Cambisol; Table 1) and reduced infiltration rates (Fig. S3) for the Luvisol, despite its sandy silty texture can be explained by its lower aggregate stability (Table 1). Runoff ratios between  $13.2 \pm 0.8 \%$  (Cambisol) and  $88.5 \pm 2.3 \%$  (Luvisol) for a  $102.8 \text{ mm h}^{-1}$  rainfall on  $0.25\text{-m}^2$  plots are comparable to those reported from a rainfall simulation experiments ( $80\text{-}85 \text{ mm h}^{-1}$  rainfall on  $0.28\text{-m}^2$  plots) in Portugal, with runoff coefficients of 7 to 55 % on Leptosols and Umbrisols (Malvar et al., 2013). Because the difference in runoff amount for the two soil types was only by a factor of seven but the erosion differed  
430 by a factor of 150 (Fig. 2a), this indicates that the higher erosion on the Luvisol is a result of the Luvisols' physical instability and susceptibility to erosion (i.e., the low aggregate stability and SOC content) and not only a result of the higher water flow (Koiter et al., 2017). Surface sealing is generally stronger for soils with a coarser soil texture and lower organic matter contents (Armenise et al., 2018). In contrast, clay-rich soils with a high physical stability (i.e., high aggregate stability) and higher TOC  
435 content are less prone to erosion, as they do not lead to rapid surface sealing and therefore slow down runoff generation and erosion (Berhe and Kleber, 2013; de Nijs and Cammeraat, 2020; Thomaz, 2018). The eroded quantities of soil ( $5.2 \pm 0.8 \text{ g m}^{-2}$ ) and TOC ( $0.32 \pm 0.04 \text{ g C m}^{-2}$ ) for the Cambisol are in the same range as for a clay-rich Alfisol ( $28 \pm 76$  to  $60 \pm 249 \text{ g m}^{-2}$ ) and TOC ( $0.9 \pm 9.8$  to  $2.2 \pm 16.2 \text{ g C m}^{-2}$ ) on  $1\text{-m}^2$  field plots (Chaplot et al., 2005). For the Luvisol, eroded quantities of soil ( $786.8$



440  $\pm 57.2 \text{ g m}^{-2}$ ) and TOC ( $29.2 \pm 2.0 \text{ g C m}^{-2}$ ) are in the same order of magnitude as for a field study conducted on loess-derived  
Luvisols in Belgium (using  $45 \text{ mm h}^{-1}$  on  $0.72\text{-m}^2$  plots), with a soil loss of  $330.2 \pm 525.6 \text{ g m}^{-2} \text{ h}^{-1}$  and a SOC loss of  $4.8 \pm$   
 $5.5 \text{ g C m}^{-2} \text{ h}^{-1}$  (Wang et al., 2010). Also Schindler Wildhaber et al. (2012) found clear differences in soil losses by runoff:  $894$   
 $\pm 282 \text{ g m}^{-2}$  for a silty soil with low SOC content ( $1.7 \pm 0.9 \%$  OC) compared to  $191 \pm 54 \text{ g m}^{-2}$  for a clay-rich soil with high  
SOC content ( $5.2 \pm 2.3 \%$  OC) under  $60 \text{ mm h}^{-1}$  for two hours in field and laboratory studies. They related the differences in  
the losses to variable soil structural stabilities and therefore susceptibility to erosion. The higher values of soil and SOC  
445 relocation in our study could partially be explained by the higher rainfall intensity ( $102.8 \text{ mm h}^{-1}$ ) since soil erosion is  
significantly correlated to rainfall intensity (Chaplot and Le Bissonnais, 2003).

Soil type is also a main explanatory variable for PyC relocation by runoff (Fig. 4a). The higher redistribution of PyC on the  
Luvisol than the Cambisol can be explained by the same processes as soil and TOC transport (i.e., rapid surface sealing, higher  
erodibility, higher runoff ratio (and thus higher sediment transport) for the Luvisol than for the Cambisol). The high runoff  
450 and transport rates on the Luvisol promoted the redistribution of the low density PyC particles on the soil surface (Abney and  
Berhe, 2018; Bird et al., 2015; Rumpel et al., 2006). Surface sealing can be increased when aggregates are broken down and  
PyC (ash and char) are washed into the soil and fill flow pathways in mechanically weaker soils (Certini, 2005; Onda et al.,  
2008). In contrast, the physical and hydrological properties of the Cambisol changed very little during the rain event, i.e. only  
 $5.2 \pm 0.8 \text{ g sediment m}^{-2}$  was recovered after 30 minutes (indicating reduced aggregate breakdown and soil loss) and soil  
455 moisture was still increasing at the end of the rainfall simulation (indicating continuous infiltration (Fig. S3)). This caused the  
seven times lower runoff and 300 times smaller PyC relocation by runoff on the Cambisol than the Luvisol.

Redistribution of soil, TOC and PyC by splash was higher for the Luvisol, but differences with the Cambisol were much  
smaller than for the transport of soil, TOC and PyC by the runoff (Fig. 2b, 3b and 4b). The measured quantities of eroded soil  
by splash ( $262.0 \pm 14.4 \text{ g m}^{-2}$  (Cambisol) and  $382.0 \pm 18.0 \text{ g m}^{-2}$  (Luvisol)) are in agreement with reported values of splashed  
460 soil for a clay loam ( $290 \pm 10 \text{ g m}^{-2}$ ) and for a silt loam ( $550 \pm 10 \text{ g m}^{-2}$ ) or sand ( $730 \pm 20 \text{ g m}^{-2}$ ) under  $30 \text{ mm h}^{-1}$  rainfall  
(Legout et al., 2005). Splash erosion, or the impact of raindrops on soil particles, is often considered the first and dominant  
process of soil detachment and transport over small distances, and depends on rainfall characteristics and soil surface properties  
(de Nijs and Cammeraat, 2020; Issa et al., 2006). The amount of splashed soil by raindrops generally increases with decreasing  
physical stability of soil (i.e. faster aggregate breakdown) and can therefore explain the larger amounts of splashed sediment  
465 for the Luvisol than the Cambisol in our study (cf., Legout et al., 2005). However, the measured quantities of eroded TOC by  
splash for the Cambisol ( $11.6 \pm 0.8 \text{ g C m}^{-2}$ ) and Luvisol ( $13.2 \pm 0.8 \text{ g C m}^{-2}$ ) were much closer than the splashed sediments,  
indicating that erosion by splash preferentially moves lighter particles (i.e. high SOC content) (Beguiría et al., 2015). In a field  
rainfall experiment in Spain, Beguiría et al. (2015) found an empirical coefficient of  $13 \text{ mg SOC relocated per g of splashed}$   
sediment, with highest SOC mobilization by splash for a sandy loam Gypsisol and lowest for a silty Cambisol. The coefficients  
470 for our study are of the same order of magnitude:  $44.3 \text{ mg TOC / g splashed sediment}$  for the Cambisol and  $34.6 \text{ mg TOC / g}$   
splashed sediment for the Luvisol. The higher coefficient for the Cambisol may be caused by the significantly higher SOC  
stock in the first 10 cm of soil ( $36.0 \pm 4.0 \text{ Mg ha}^{-1}$  for the Cambisol vs  $23.4 \pm 0.2 \text{ Mg ha}^{-1}$  for the Luvisol; Table 1).



Soil type also influenced PyC translocation by splash (Fig. 4b). The smaller difference between the two soil types indicates that PyC erosion by splash depends much less on soil type than it did for runoff. Splash preferentially moves lighter particles  
475 (Beguería et al., 2015). Along the argumentation above for TOC, this effect can be related to the fact that PyC was available on the soil surface of both soils and the physical properties of PyC, such as the low density.

Finally, soil type was the main explanatory variable for vertical movement of PyC through the 10 cm soil column (Fig. 6). We found more PyC at 3-10 cm depth in the Cambisol than the Luvisol at the upslope position where PyC was initially added, as well as in the subsurface along the slope gradient. The higher vertical and subsurface mobility of PyC in the Cambisol  
480 compared to the Luvisol under unsaturated conditions (and excluding leaching of soluble parts) can be explained by higher infiltration rates for the Cambisol with high aggregate stability (Table 1 and Fig. S3). Therefore, more PyC was physically translocated (i.e. as particulate PyC or clay-sized PyC) with the percolating water running through larger soil pores (Hilscher and Knicker, 2011; Rumpel et al., 2015; Soucémarianadin et al., 2019). This vertical transport was limited in the Luvisol due to quicker surface sealing. The vertical movement of PyC depends largely on PyC size and solubility, but also on soil properties  
485 such as texture, aggregation, porosity and the infiltration rate (Abney et al., 2017), which in our study were more favourable in the Cambisol.

#### 4.3.2 PyC characteristics

PyC characteristics (feedstock and particle size) was the second most important explanatory variable affecting PyC redistribution. For PyC feedstock, however, we found contradictory results, in particular for wood-PyC. On the one hand, there  
490 was more wood-PyC transport by runoff and splash (sediment + floating particles) than grass-PyC transport for both soils (% of total added PyC:  $43.4 \pm 6.6$  % for wood-PyC and  $28.4 \pm 4.6$  % for grass-PyC; Fig. 4). On the other hand, we also found more wood-PyC than grass-PyC on the soil surface (0-1 cm) in the upslope position where PyC was applied for both soils (fraction of OC derived from the PyC in % (or PyC fraction):  $11.5 \pm 1.5$  % for wood-PyC and  $7.4 \pm 1.0$  % for grass-PyC; Fig. 6a-b), indicating that wood-PyC either remained where initially applied or moved outside the 0.25-m<sup>2</sup> plot, while grass-PyC  
495 was redistributed more within the plot. The latter observation is in line with the general concept that grass-derived PyC has greater mobility than wood-derived PyC, which remains closer to its site of formation and initial deposition (Saiz et al., 2018). The higher mobility of grass-PyC could be explained by its higher fragmentation potential due to the lack of strong physical structures of grass feedstock compared to wood feedstock (Pignatello et al., 2015; Singh et al., 2012). Wood feedstock is generally richer in lignin, and the resulting wood-PyC is more crystalline and aromatic (Keiluweit et al., 2010; Singh et al.,  
500 2012), which was also the case for our PyC (Fig. S1). These differences can explain the higher retention of wood-PyC compared to grass-PyC on the soil surface at the upslope position of the plots, but not the greater relocation of wood-PyC than grass-PyC by runoff and splash. We assume that this is caused by the greater fragmentation of grass-PyC into smaller particles by raindrop impact. These smaller particles are more easily distributed in the soil, which make them more difficult to detect based on  $\delta^{13}\text{C}$  and the proportion of PyC (few g) to soil (several kg) (McCorkle et al., 2016; Pignatello et al., 2015). Overall,  
505 we found much more of the applied wood-PyC than the grass-PyC, both PyC recoveries (% of total added PyC:  $43.4 \pm 6.6$  %



for wood-PyC and  $28.4 \pm 4.6$  % for grass-PyC; Fig. 4) and PyC fraction (fraction of OC derived from the PyC in %:  $26.9 \pm 4.9$  % for wood-PyC and  $17.7 \pm 3.8$  % for grass-PyC; Fig. 6), which supports this assumption. It has also been shown that PyC derived from wood physically disintegrates quicker than PyC derived from other sources, such as grass, which could explain why more wood-PyC was relocated by runoff and splash (Spokas et al., 2014). Our different findings ultimately indicate that  
510 both the fragmentation potential, as well as the mobility of PyC do not only depend on the feedstock material (grass versus wood) but also other factors such as surface area, porosity, induced mechanical stresses, etc. (Crawford and Belcher, 2014; Singh et al., 2012; Spokas et al., 2014).

For the runoff and splashed sediment (without floating particles), the mobility of fine PyC particles was larger than for the coarse particles (Fig. 4a-b). This finding is in line with the greater retention of coarse PyC particles on the soil surface (0-1 cm) in the upper part of the plot where PyC was added, especially for the Cambisol (Fig. 6a-b). Particle size can be a key driver of  
515 long-distance transport of PyC. It is generally assumed that the surface transport potential and efficiency is greater for finer PyC particles and they are therefore transported over longer distances (off-site export) than coarser particles that remain closer to the site of formation (Abiven and Santín, 2019; Masiello, 2004; Saiz et al., 2018; Tinner et al., 2006). Finer PyC particles also remain in suspension for a longer period of time as they settle from the mixture slower (according to Fick's law) (Rumpel et al., 2015). Since the particle size determines PyC susceptibility to erosive transport, fragmentation after initial deposition  
520 (and during transport) can increase the transport potential of PyC particles. Higher fragmentation of grass-PyC into smaller particles could ultimately lead to higher mobility (Pignatello et al., 2015; Rumpel et al., 2015). Only for the separated floating particles eroded by runoff and splash (Fig. 4c-d), were the coarse PyC particles more prevalent. The larger quantities of coarse PyC in the floating particles of runoff and splash are caused by the higher floating potential of coarser PyC, likely due to its  
525 low density and high porosity (Rumpel et al., 2015).

#### 4.3.3 Slope

Slope angle had a minor effect on the mobilized quantities of soil, SOC and PyC and was only significant for the Luvisol, where a slope of  $25^\circ$  resulted in increased soil and TOC, but not PyC erosion by runoff (Fig. 2-4). As slope was only relevant for the Luvisol and only for particles transported by runoff, it could be related to the greater runoff ratio and therefore surface  
530 transport for the Luvisol under a  $25^\circ$  slope. Several studies have confirmed the limited effect of slope on PyC redistribution (Boot et al., 2015; Cotrufo et al., 2016; Galanter et al., 2018), but it is important to note that slope angle may be more important on larger plots or along hillslopes where slope angle can be assessed together with slope length and aspect (Abney and Berhe, 2018; Shakesby et al., 2015). These two topographic features could not be assessed in our plot-scale study.

#### 4.4 Consequences for understanding PyC redistribution in the landscape after fire

535 Our findings regarding the factors that affect PyC relocation during simulated rainfall events advance our understanding of PyC redistribution in the landscape. We show that PyC was highly mobile, and quickly transported and relocated on  $0.25\text{-m}^2$  plots during 30 minutes of intense rainfall. Our experimental study was done under controlled conditions, which partially limits



a direct comparison of our data to natural hillslopes. To fully understand PyC redistribution and deposition in the landscape after a fire, it is therefore of great importance to assess initial post-fire rainfall events and to track PyC relocation by erosion at the hillslope and catchment scales (Cotrufo et al., 2016; Masiello and Berhe, 2020). In particular, the plots used in this study are much shorter than real hillslopes and therefore do not account for long-distance transport (Rumpel et al., 2006). For longer hillslopes, slope steepness, length and aspect, post-fire surface roughness, but also micro-topographic features such as depressions, or the formation of rills and gullies affect the effective infiltration rates and transport capacity of overland flow, and thus runoff erosion and PyC redistribution. With increasing hillslope steepness and decreasing surface roughness (due to removal of ground cover after a fire), surface runoff and PyC transport will likely increase; with increasing hillslope length, the transport capacity of overland flow generally declines, which increases the chances that PyC is deposited along the slope or in lower-lying areas of catchments and can ultimately enter the soil (Abney and Berhe, 2018; Masiello and Berhe, 2020). In addition, the results will be different for real post-fire landscapes because of the heterogeneity in ground cover and soil hydrological and physical properties of fire-affected (burned) soils. Fire-affected soils are affected by changes in i.e. vegetation cover, hydrophobicity, water repellence, infiltration or aggregate breakdown (Abney and Berhe, 2018; Moody et al., 2013; Shakesby, 2011). The fire regime (severity, intensity and frequency) will determine the fuel consumption, as well as PyC production and characteristics (Bowman et al., 2009; Santín et al., 2015). In our experiment, we used unburnt soil without ground cover except for the added PyC. Fires remove substantial proportions of ground cover (up to 90 %), but after an actual fire the soil surface may be covered with debris, ash, charcoal or partially burned plant material, which will lead to a patchy ground cover (Johansen et al., 2001; Pierson et al., 2013; Shakesby and Doerr, 2006). In our study, both the soils (very hydrophilic) and PyC materials (extremely hydrophobic) were similarly water repellent (Table 1-2). On real fire-affected hillslopes, burnt soils will likely be more water repellent, leading to more runoff and likely more transport of particles and PyC (DeBano, 2000). Fires can also change the water holding capacity of soils and soil chemistry (Fonseca et al., 2017; Moragues-Saitua et al., 2017; Robichaud et al., 2016). However, we did not change the soils physical structure (i.e. aggregation or porosity) prior to rainfall experiments, except that we slightly smoothed the surface. Burned soils may strongly be affected by changes in aggregation, porosity and therefore infiltration capacity due to heat-induced aggregate breakdown, volatilisation or charring of organic matter or in-wash of particles, such as ash or PyC, resulting in i.e. more pore clogging and surface sealing than in our experiment (Certini, 2005; Jian et al., 2018). However, limited clogging through in wash of ash or PyC has also been found (Stoof et al., 2016). Even though we did not account for these changes in fire-affected soils, our results of PyC redistribution are relatively comparable with plot-scale studies using burnt soils in the field (Rumpel et al., 2009). Precipitation also has a great influence on post-fire erosion dynamics, but is highly variable in nature, and depends on local to regional climatic conditions. Although rainfall simulation experiments on plots are essential to understand individual processes during single erosion events due to high level of control and comparability, they are limited in spatial and temporal extend (Clarke and Walsh, 2007; Doetterl et al., 2016; Iserloh et al., 2012). PyC redistribution after rainfall will not be uniform in time and space, and it is therefore important to use multiple successive events in future studies to take this temporal and spatial evolution into account (Moody et al., 2013). Using longer rainfall durations or successive rainfall events would likely have



575 resulted in parts of the remaining PyC on the soil surface to be further relocated by runoff and splash, but probably to a much lesser extent. Longer rainfall events could facilitate redistribution of PyC that had already entered the soil column after 30 minutes. A lower rainfall intensity would likely have led to less overland flow and reduced transport by runoff, but possibly still substantial PyC redistribution due to preferential relocation of low-density particles like PyC. An even higher rainfall intensity would likely have led to more overland flow, and increased sediment and PyC transport (Moody et al., 2013; Rumpel et al., 2015). Higher rainfall intensities or longer durations could likely further facilitate breakdown of PyC particles due to the impact of the raindrops, subsequently increasing its mobility.

580 Despite the limitations of these experimental settings, controlled conditions and multi-factorial experiments are crucial for our understanding of key drivers of PyC redistribution. The data and findings of this study give directions for larger-scale field studies and help generalization of model parameters. In particular, our results clearly show that soil type affects the mobility of PyC. PyC export is less for a fine-textured well-aggregated soil than for silty soil with poorer aggregate stability. This result is in line with the notion that soil properties, together with key hydrological drivers, determine the spatial variability of PyC in soils at the landscape scale (Rumpel et al., 2009; Soucémariadin et al., 2019). Our findings indicate that PyC redistribution  
585 depends on the feedstock from which it was derived. Both wood- and grass-PyC can be highly mobile, depending, at least partially, on its particle size. PyC relocation may be greater for grassland-dominated than tree-dominated catchments because grass-PyC is smaller and more susceptible to fragmentation, therefore potentially breaking apart into even smaller pieces that are more mobile (Pignatello et al., 2015; Saiz et al., 2018). Consequently, vegetation cover determines the feedstock for PyC production, which in turn will likely govern the size, stability and therefore mobility of PyC (Saiz et al., 2018). This needs to  
590 be taken into account for field investigations and for modelling of PyC erosion at the hillslope or catchment scale. In addition, our results suggest that the presence and redistribution of PyC in the landscape can affect soil organic matter mobilization. We showed that nSOC export changes in the presence of PyC, but the processes that cause these changes could not be assessed and need further study.

## 5 Conclusions

595 The rainfall simulation experiment on 0.25-m<sup>2</sup> soil plots presented here show that large quantities of PyC can be redistributed during a short period of time. Between  $3.7 \pm 1.0$  % to  $73.4 \pm 3.8$  % of the initially added PyC was redistributed by runoff and splash during a 30 minute high intensity rainfall event. Soil texture, slope angle, PyC feedstock and particle size affect the mobilization of PyC to a different extent. Soil type substantially influences the redistribution of PyC at the plot scale, probably due to differences in texture, aggregate stability, and SOC contents. For the studied Cambisol, only little PyC was moved with  
600 runoff or splash and significantly more PyC remained on the plot where it was initially applied or moved vertically into the soil. For the Luvisol, large quantities of PyC were moved with runoff and splash, but only little PyC moved vertically into the soil column. Furthermore, the erosional behaviour of wood- and grass-PyC differed, suggesting that this must be taken into account when determining post-fire erosion budgets for catchments under different vegetation. While more wood-PyC was



605 mobilised by runoff and splash than grass-PyC, also more wood-PyC was retained on the surface where it was initially applied. Alongside PyC feedstock, particle size also influences the mobility and off-site transport of PyC. Relocation of PyC may be greater for grass-dominated ecosystems because grass-PyC is initially smaller and also more susceptible to fragmentation; the finer PyC is, the more susceptible to redistribution. Slope angle had only a minor effect on PyC relocation at the plot scale but must be taken into account for larger scales, such as hillslopes or catchments. Finally, the presence and relocation of PyC affected the mobilization and export of native SOC.

610 The identification of the relative importance of these individual drivers of PyC redistribution will help to improve the design of more time- and cost-intensive field studies. Our simulation experiments can also provide crucial inputs to simulate the fate of PyC in landscape or Earth system models. However, further research is needed to understand the importance of key drivers of PyC redistribution at larger scales, such as hillslopes or catchments, in order to explain the spatial heterogeneity of SOC and PyC stocks in the landscape.

#### 615 **Authors' contribution**

SA raised the funding. SB and SA conceptualized the study. SB conducted the experiment, analysed and visualised the data and wrote the manuscript and all authors commented on the manuscript.

#### **Competing interests**

The authors declare that they have no conflict of interest.

#### 620 **Acknowledgment**

The authors acknowledge the support and ability to use the facilities at the Swiss Federal Institute for Forest, Snow and Landscape Research (WSL), especially Dr. Manfred Staehli and Werner Gerber. We further thank Thomas Keller (University of Zurich) for technical assistance. The study was funded by the Swiss National Science Foundation (project no. 200021\_178768)

#### 625 **References**

- Abd Elbasit, M.A.M., Yasuda, H., Salmi, A., Anyoji, H., 2010. Characterization of rainfall generated by dripper-type rainfall simulator using piezoelectric transducers and its impact on splash soil erosion. *Earth Surface Processes and Landforms* 35, 466–475. doi:10.1002/esp.1935
- Abiven, S., Santín, C., 2019. Editorial: From Fires to Oceans: Dynamics of Fire-Derived Organic Matter in Terrestrial and Aquatic Ecosystems. *Frontiers in Earth Science* 7, 1–4. doi:10.3389/feart.2019.00031
- 630



- Abney, R.B., Berhe, A.A., 2018. Pyrogenic Carbon Erosion: Implications for Stock and Persistence of Pyrogenic Carbon in Soil. *Frontiers in Earth Science* 6, 1–16. doi:10.3389/feart.2018.00026
- Abney, R.B., Jin, L., Berhe, A.A., 2019a. Soil properties and combustion temperature: Controls on the decomposition rate of pyrogenic organic matter. *Catena* 182, 104127. doi:10.1016/j.catena.2019.104127
- 635 Abney, R.B., Kuhn, T.J., Chow, A., Hockaday, W., Fogel, M.L., Berhe, A.A., 2019b. Pyrogenic carbon erosion after the Rim Fire, Yosemite National Park: the role of burn severity and slope. *Journal of Geophysical Research: Biogeosciences* 124, 1–18. doi:10.1029/2018jg004787
- Abney, R.B., Sanderman, J., Johnson, D., Fogel, M.L., Berhe, A.A., 2017. Post-wildfire Erosion in Mountainous Terrain Leads to Rapid and Major Redistribution of Soil Organic Carbon. *Frontiers in Earth Science* 5, 1–16.  
640 doi:10.3389/feart.2017.00099
- Abudi, I., Carmi, G., Berliner, P., 2012. Rainfall simulator for field runoff studies. *Journal of Hydrology* 454–455, 76–81. doi:10.1016/j.jhydrol.2012.05.056
- Aksoy, H., Unal, N.E., Cokgor, S., Gedikli, A., Yoon, J., Koca, K., Inci, S.B., Eris, E., 2012. A rainfall simulator for laboratory-scale assessment of rainfall-runoff-sediment transport processes over a two-dimensional flume. *Catena* 98,  
645 63–72. doi:10.1016/j.catena.2012.06.009
- Archibald, S., Lehmann, C.E.R., Gómez-Dans, J.L., Bradstock, R.A., 2013. Defining pyromes and global syndromes of fire regimes. *Proceedings of the National Academy of Sciences of the United States of America* 110, 6442–6447.
- Armenise, E., Simmons, R.W., Ahn, S., Garbout, A., Doerr, S.H., Mooney, S.J., Sturrock, C.J., Ritz, K., 2018. Soil seal development under simulated rainfall: Structural, physical and hydrological dynamics. *Journal of Hydrology* 556, 211–  
650 219. doi:10.1016/j.jhydrol.2017.10.073
- Beguiría, S., Angulo-Martínez, M., Gaspar, L., Navas, A., 2015. Detachment of soil organic carbon by rainfall splash: Experimental assessment on three agricultural soils of Spain. *Geoderma* 245–246, 21–30. doi:10.1016/j.geoderma.2015.01.010
- Berger, C., Schulze, M., Rieke-Zapp, D., Schlunegger, F., 2010. Rill development and soil erosion: A laboratory study of  
655 slope and rainfall intensity. *Earth Surface Processes and Landforms* 35, 1456–1467. doi:10.1002/esp.1989
- Berhe, A.A., Barnes, R.T., Six, J., Marín-Spiotta, E., 2018. Role of Soil Erosion in Biogeochemical Cycling of Essential Elements: Carbon, Nitrogen, and Phosphorus. *Annual Review of Earth and Planetary Sciences* 46, 521–548. doi:10.1146/annurev-earth-082517-010018
- Berhe, A.A., Harden, J.W., Torn, M.S., Kleber, M., Burton, S.D., Harte, J., 2012. Persistence of soil organic matter in eroding versus depositional landform positions. *Journal of Geophysical Research: Biogeosciences* 117, 1–16.  
660 doi:10.1029/2011JG001790
- Berhe, A.A., Harte, J., Harden, J.W., Torn, M.S., 2007. The Significance of the Erosion-induced Terrestrial Carbon Sink. *BioScience* 57, 337. doi:10.1641/B570408
- Berhe, A.A., Kleber, M., 2013. Erosion, deposition, and the persistence of soil organic matter: Mechanistic considerations



- 665 and problems with terminology. *Earth Surface Processes and Landforms* 38, 908–912. doi:10.1002/esp.3408
- Bird, M.I., Wynn, J.G., Saiz, G., Wurster, C.M., McBeath, A., 2015. The Pyrogenic Carbon Cycle. *Annual Review of Earth and Planetary Sciences* 43, 273–298. doi:10.1146/annurev-earth-060614-105038
- Boot, C.M., Haddix, M., Paustian, K., Cotrufo, M.F., 2015. Distribution of black carbon in ponderosa pine forest floor and soils following the High Park wildfire. *Biogeosciences* 12, 3029–3039. doi:10.5194/bg-12-3029-2015
- 670 Bowman, D.M.J.S., Balch, J.K., Artaxo, P., Bond, W.J., Carlson, J.M., Cochrane, M.A., D’Antonio, C.M., DeFries, R.S., Doyle, J.C., Harrison, S.P., Johnston, F.H., Keeley, J.E., Krawchuk, M.A., Kull, C.A., Marston, J.B., Moritz, M.A., Prentice, I.C., Roos, C.I., Scott, A.C., Swetnam, T.W., van der Werf, G.R., Pyne, S.J., 2009. Fire in the Earth System. *Science* 324, 481–484. doi:10.1126/science.1163886
- Braun, S., Tresch, S., Augustin, S., 2020. Soil solution in Swiss forest stands: A 20 year’s time series. *PloS One* 15, e0227530. doi:10.1371/journal.pone.0227530
- 675 Brewer, C.E., Chuang, V.J., Masiello, C.A., Gonnermann, H., Gao, X., Dugan, B., Driver, L.E., Panzacchi, P., Zygourakis, K., Davies, C.A., 2014. New approaches to measuring biochar density and porosity. *Biomass and Bioenergy* 66, 176–185. doi:10.1016/j.biombioe.2014.03.059
- Certini, G., 2005. Effects of fire on properties of forest soils: a review. *Oecologia* 143, 1–10. doi:10.1007/s00442-004-1788-8
- 680 Chaplot, V., Le Bissonnais, Y., 2003. Runoff features for interrill erosion at different rainfall intensities, slope lengths, and gradients in an agricultural loessial hillslope. *Soil Science Society of America Journal* 67, 844–851. doi:10.2136/sssaj2003.8440
- Chaplot, V., Le Bissonnais, Y., Bernadou, J., 2005. Runoff, soil and soil organic carbon losses within a small sloping-land catchment of Laos under shifting cultivation. *Advances in Soil Science* 263–276.
- 685 Chappell, A., Baldock, J., Sanderman, J., 2016. The global significance of omitting soil erosion from soil organic carbon cycling schemes. *Nature Climate Change* 6, 187–191. doi:10.1038/nclimate2829
- Chatterjee, S., Santos, F., Abiven, S., Itin, B., Stark, R.E., Bird, J.A., 2012. Elucidating the chemical structure of pyrogenic organic matter by combining magnetic resonance, mid-infrared spectroscopy and mass spectrometry. *Organic Geochemistry* 51, 35–44. doi:10.1016/j.orggeochem.2012.07.006
- 690 Christiansen, J.E., 1942. Irrigation by Sprinkling - Bulletin 670. University of California, College of Agriculture, Agricultural Experiment Station, Berkeley, California.
- Chrzaszvez, J., Théry-Parisot, I., Fiorucci, G., Terral, J.F., Thibaut, B., 2014. Impact of post-depositional processes on charcoal fragmentation and archaeobotanical implications: Experimental approach combining charcoal analysis and biomechanics. *Journal of Archaeological Science* 44, 30–42. doi:10.1016/j.jas.2014.01.006
- 695 Clarke, M.A., Walsh, R.P.D., 2007. A portable rainfall simulator for field assessment of splash and slopewash in remote locations. *Earth Surface Processes and Landforms* 32, 2052–2069. doi:10.1002/esp
- Conard, S.G., Solomon, A.M., 2009. Effect of wildland fire on regional and global carbon stocks in a changing environment,



- in: Bytnerowicz, A., Arbaugh, M., Riebau, A., Andersen, C. (Eds.), *Developments in Environmental Science*. Elsevier  
700 B.V., pp. 109–138. doi:10.1016/S1474-8177(08)00005-3
- Coppola, A.I., Druffel, E.R.M., 2016. Cycling of black carbon in the ocean. *Geophysical Research Letters* 43, 4477–4482.  
doi:10.1002/2016GL068574
- Cotrufo, M.F., Boot, C., Kampf, S., Nelson, P.A., Brogan, D.J., Covino, T., Haddix, M., MacDonald, L.H., Rathburn, S.,  
705 Ryan-Bukett, S., Schmeer, S., Hall, E., 2016. Redistribution of pyrogenic carbon from hillslopes to stream corridors  
following a large montane wildfire. *Global Biogeochemical Cycles* 30, 1348–1355. doi:10.1111/1462-2920.13280
- Crawford, A.J., Belcher, C.M., 2014. Charcoal Morphometry for Paleocological Analysis: The Effects of Fuel Type and  
Transportation on Morphological Parameters. *Applications in Plant Sciences* 2, 1400004. doi:10.3732/apps.1400004
- de Nijs, E.A., Cammeraat, E.L.H., 2020. The stability and fate of Soil Organic Carbon during the transport phase of soil  
erosion. *Earth-Science Reviews* 201. doi:10.1016/j.earscirev.2019.103067
- 710 DeBano, L.F., 2000. The role of fire and soil heating on water repellency in wildland environments: a review. *Journal of  
Hydrology* 231–232, 195–206.
- Doerr, S.H., 1998. On standardizing the “water drop penetration time” and the “molarity of an ethanol droplet” techniques to  
classify soil hydrophobicity: a case study using medium textured soils. *Earth Surface Processes and Landforms* 23,  
663–668. doi:10.1002/(SICI)1096-9837(199807)23:7<663::AID-ESP909>3.0.CO;2-6
- 715 Doetterl, S., Berhe, A.A., Nadeu, E., Wang, Z., Sommer, M., Fiener, P., 2016. Erosion, deposition and soil carbon: A review  
of process-level controls, experimental tools and models to address C cycling in dynamic landscapes. *Earth-Science  
Reviews* 154, 102–122. doi:10.1016/j.earscirev.2015.12.005
- Federal Office of Meteorology and Climatology, MeteoSwiss, 2019. Swiss climate in detail. Extreme value analysis (version  
2019). [https://www.meteoswiss.admin.ch/home/climate/swiss-climate-in-detail/extreme-value-analyses/standard-](https://www.meteoswiss.admin.ch/home/climate/swiss-climate-in-detail/extreme-value-analyses/standard-period.html)  
720 [period.html](https://www.meteoswiss.admin.ch/home/climate/swiss-climate-in-detail/extreme-value-analyses/standard-period.html)? (last access: 29. September 2020)
- Fonseca, F., de Figueiredo, T., Nogueira, C., Queirós, A., 2017. Effect of prescribed fire on soil properties and soil erosion in  
a Mediterranean mountain area. *Geoderma* 307, 172–180. doi:10.1016/j.geoderma.2017.06.018
- Galanter, A., Cadol, D., Lohse, K., 2018. Geomorphic influences on the distribution and accumulation of pyrogenic carbon  
(PyC) following a low severity wildfire in northern New Mexico. *Earth Surface Processes and Landforms* 43, 2207–  
725 2218. doi:10.1002/esp.4386
- Giglio, L., Randerson, J.T., Van Der Werf, G.R., 2013. Analysis of daily, monthly, and annual burned area using the fourth-  
generation global fire emissions database (GFED4). *Journal of Geophysical Research: Biogeosciences* 118, 317–328.  
doi:10.1002/jgrg.20042
- Güereña, D.T., Lehmann, J., Walter, T., Enders, A., Neufeldt, H., Odiwour, H., Biwott, H., Recha, J., Shepherd, K., Barrios,  
730 E., Wurster, C., 2015. Terrestrial pyrogenic carbon export to fluvial ecosystems: Lessons learned from the White Nile  
watershed of East Africa. *Global Biogeochemical Cycles* 29, 1911–1928. doi:10.1002/2015GB005095. Received
- Hagedorn, F.H., Spinnler, D., Bundt, M., Blaser, P., Siegwolf, R., 2003. The input and fate of new C in two forest soils



- under elevated CO<sub>2</sub>. *Global Change Biology* 9, 862–872. doi:10.1046/j.1365-2486.2003.00638.x
- 735 Hammes, K., Abiven, S., 2013. Identification of Black Carbon in the Earth System, in: *Fire Phenomena and the Earth System: An Interdisciplinary Guide to Fire Science*. pp. 157–176. doi:10.1002/9781118529539.ch9
- Hammes, K., Smernik, R.J., Skjemstad, J.O., Herzog, A., Vogt, U.F., Schmidt, M.W.I., 2006. Synthesis and characterisation of laboratory-charred grass straw (*Oryza sativa*) and chestnut wood (*Castanea sativa*) as reference materials for black carbon quantification. *Organic Geochemistry* 37, 1629–1633. doi:10.1016/j.orggeochem.2006.07.003
- 740 Hilber, I., Blum, F., Leifeld, J., Schmidt, H.P., Bucheli, T.D., 2012. Quantitative determination of PAHs in biochar: A prerequisite to ensure its quality and safe application. *Journal of Agricultural and Food Chemistry* 60, 3042–3050. doi:10.1021/jf205278v
- Hilscher, A., Knicker, H., 2011. Degradation of grass-derived pyrogenic organic material, transport of the residues within a soil column and distribution in soil organic matter fractions during a 28month microcosm experiment. *Organic Geochemistry* 42, 42–54. doi:10.1016/j.orggeochem.2010.10.005
- 745 Iserloh, T., Fister, W., Seeger, M., Willger, H., Ries, J.B., 2012. A small portable rainfall simulator for reproducible experiments on soil erosion. *Soil and Tillage Research* 124, 131–137. doi:10.1016/j.still.2012.05.016
- Issa, O.M., Bissonnais, Y. Le, Planchon, O., Favis-Mortlock, D., Silvera, N., Wainwright, J., 2006. Soil detachment and transport on field- and laboratory-scale interrill areas: Erosion processes and the size-selectivity of eroded sediment. *Earth Surface Processes and Landforms* 31, 929–939. doi:10.1002/esp.1303
- 750 IUSS Working Group WRB, 2015. *World Reference Base for Soil Resources 2014, update 2015*. International soil classification systems for naming soils and creating legends for soil maps., World Soil Resources Reports No. 106. FAO, Rome.
- Jian, M., Berhe, A.A., Berli, M., Ghezzehei, T.A., 2018. Vulnerability of physically protected soil organic carbon to loss under low severity fires. *Frontiers in Environmental Science* 6, 1–12. doi:10.3389/fenvs.2018.00066
- 755 Jiang, X., Haddix, M.L., Cotrufo, M.F., 2016. Interactions between biochar and soil organic carbon decomposition: Effects of nitrogen and low molecular weight carbon compound addition. *Soil Biology and Biochemistry* 100, 92–101. doi:10.1016/j.soilbio.2016.05.020
- Jiang, X., Tan, X., Cheng, J., Haddix, M.L., Cotrufo, M.F., 2019. Interactions between aged biochar, fresh low molecular weight carbon and soil organic carbon after 3.5 years soil-biochar incubations. *Geoderma* 333, 99–107. doi:10.1016/j.geoderma.2018.07.016
- 760 Johansen, M.P., Hakonson, T.E., Breshears, D.D., 2001. Post-fire runoff and erosion from rainfall simulation: Contrasting forests with shrublands and grasslands. *Hydrological Processes* 15, 2953–2965. doi:10.1002/hyp.384
- Jones, M.W., Santín, C., van der Werf, G.R., Doerr, S.H., 2019. Global fire emissions buffered by the production of pyrogenic carbon. *Nature Geoscience* 12, 742–747. doi:10.1038/s41561-019-0403-x
- 765 Kathiravelu, G., Lucke, T., Nichols, P., 2016. Rain drop measurement techniques: A review. *Water (Switzerland)* 8. doi:10.3390/w8010029



- Keiluweit, M., Nico, P.S., Johnson, M., Kleber, M., 2010. Dynamic molecular structure of plant biomass-derived black carbon (biochar). *Environmental Science and Technology* 44, 1247–1253. doi:10.1021/es9031419
- 770 Koiter, A.J., Owens, P.N., Peticrew, E.L., Lobb, D.A., 2017. The role of soil surface properties on the particle size and carbon selectivity of interrill erosion in agricultural landscapes. *Catena* 153, 194–206. doi:10.1016/j.catena.2017.01.024
- Lal, R., 2004. Soil Carbon Sequestration Impacts on Global Climate Change and Food Security. *Science* 304, 1623–1627.
- Lasslop, G., Coppola, A.I., Voulgarakis, A., Yue, C., Veraverbeke, S., 2019. Influence of Fire on the Carbon Cycle and Climate. *Current Climate Change Reports*. doi:10.1007/s40641-019-00128-9
- 775 Lassu, T., Seeger, M., 2015. Set-up and calibration of an indoor nozzle-type rainfall simulator for soil erosion studies. *Land Degradation and Development* 26, 604–612. doi:10.1002/ldr.2360
- Le Bissonnais, Y., 2016. Aggregate stability and assessment of soil crustability and erodibility: I. Theory and methodology. *European Journal of Soil Science* 67, 11–21. doi:10.1111/ejss.4\_12311
- Legout, C., Leguédois, S., Le Bissonnais, Y., Malam Issa, O., 2005. Splash distance and size distributions for various soils. 780 *Geoderma* 124, 279–292. doi:10.1016/j.geoderma.2004.05.006
- Maestrini, B., Abiven, S., Singh, N., Bird, J., Torn, M.S., Schmidt, M.W.I., 2014. Carbon losses from pyrolysed and original wood in a forest soil under natural and increased N deposition. *Biogeosciences* 11, 5199–5213. doi:10.5194/bg-11-5199-2014
- Major, J., Lehmann, J., Rondon, M., Goodale, C., 2010. Fate of soil-applied black carbon: Downward migration, leaching 785 and soil respiration. *Global Change Biology* 16, 1366–1379. doi:10.1111/j.1365-2486.2009.02044.x
- Malvar, M.C., Martins, M.A.S., Nunes, J.P., Robichaud, P.R., Keizer, J.J., 2013. Assessing the role of pre-fire ground preparation operations and soil water repellency in post-fire runoff and inter-rill erosion by repeated rainfall simulation experiments in Portuguese eucalypt plantations. *Catena* 108, 69–83. doi:10.1016/j.catena.2012.11.004
- Masiello, C.A., 2004. New directions in black carbon organic geochemistry. *Marine Chemistry* 92, 201–213. 790 doi:10.1029/2002GB001939
- Masiello, C.A., Berhe, A.A., 2020. First Interactions with the Hydrologic Cycle Determine Pyrogenic Carbon's Fate in the Earth System. *Earth Surface Processes and Landforms*. doi:10.1002/esp.4925
- McCorkle, E.P., Berhe, A.A., Hunsaker, C.T., Johnson, D.W., McFarlane, K.J., Fogel, M.L., Hart, S.C., 2016. Tracing the source of soil organic matter eroded from temperate forest catchments using carbon and nitrogen isotopes. 795 *Chemical Geology* 445, 172–184. doi:10.1016/j.chemgeo.2016.04.025
- Moody, J.A., Shakesby, R.A., Robichaud, P.R., Cannon, S.H., Martin, D.A., 2013. Current research issues related to post-wildfire runoff and erosion processes. *Earth-Science Reviews* 122, 10–37. doi:10.1016/j.earscirev.2013.03.004
- Moragues-Saitua, L., Arias-González, A., Gartzia-Bengoetxea, N., 2017. Effects of biochar and wood ash on soil hydraulic properties: A field experiment involving contrasting temperate soils. *Geoderma* 305, 144–152. 800 doi:10.1016/j.geoderma.2017.05.041



- Onda, Y., Dietrich, W.E., Booker, F., 2008. Evolution of overland flow after a severe forest fire, Point Reyes, California. *Catena* 72, 13–20. doi:10.1016/j.catena.2007.02.003
- Pierson, F.B., Jason Williams, C., Hardegee, S.P., Clark, P.E., Kormos, P.R., Al-Hamdan, O.Z., 2013. Hydrologic and erosion responses of sagebrush steppe following juniper encroachment, wildfire, and tree cutting. *Rangeland Ecology and Management* 66, 274–289. doi:10.2111/REM-D-12-00104.1
- 805 Pignatello, J.J., Uchimiya, M., Abiven, S., Schmidt, M.W.I., 2015. Evolution of biochar properties in soil, in: *Biochar for Environmental Management*. pp. 195–233. doi:10.4324/9780203762264-16
- Poepflau, C., Vos, C., Don, A., 2017. Soil organic carbon stocks are systematically overestimated by misuse of the parameters bulk density and rock fragment content. *Soil* 3, 61–66. doi:10.5194/soil-3-61-2017
- 810 Proulx, R., Rheault, G., Bonin, L., Roca, I.T., Martin, C.A., Desrochers, L., Seiferling, I., 2015. How much biomass do plant communities pack per unit volume? *PeerJ* 3, 1–10. doi:10.7717/peerj.849
- Pyle, L.A., Magee, K.L., Gallagher, M.E., Hockaday, W.C., Masiello, C.A., 2017. Short-Term Changes in Physical and Chemical Properties of Soil Charcoal Support Enhanced Landscape Mobility. *Journal of Geophysical Research: Biogeosciences* 122, 3098–3107. doi:10.1002/2017JG003938
- 815 Randerson, J.T., Chen, Y., Van Der Werf, G.R., Rogers, B.M., Morton, D.C., 2012. Global burned area and biomass burning emissions from small fires. *Journal of Geophysical Research G: Biogeosciences* 117. doi:10.1029/2012JG002128
- R Core Team, 2018. R: A language and environment for statistical computing. R Foundation for Statistical Computing, Vienna, Austria. URL <https://www.R-project.org/>.
- Reisser, M., Purves, R.S., Schmidt, M.W.I., Abiven, S., 2016. Pyrogenic Carbon in Soils: A Literature-Based Inventory and a Global Estimation of Its Content in Soil Organic Carbon and Stocks. *Frontiers in Earth Science* 4, 1–14. doi:10.3389/feart.2016.00080
- 820 Robichaud, P.R., Wagenbrenner, J.W., Pierson, F.B., Spaeth, K.E., Ashmun, L.E., Moffet, C.A., 2016. Infiltration and interrill erosion rates after a wildfire in western Montana, USA. *Catena* 142, 77–88. doi:10.1016/j.catena.2016.01.027
- Ruehr, N.K., Knohl, A., Buchmann, N., 2010. Environmental variables controlling soil respiration on diurnal, seasonal and annual time-scales in a mixed mountain forest in Switzerland. *Biogeochemistry* 98, 153–170. doi:10.1007/s10533-009-9383-z
- 825 Rumpel, C., Ba, A., Darboux, F., Chaplot, V., Planchon, O., 2009. Erosion budget and process selectivity of black carbon at meter scale. *Geoderma* 154, 131–137. doi:10.1016/j.geoderma.2009.10.006
- Rumpel, C., Chaplot, V., Planchon, O., Bernadou, J., Valentin, C., Mariotti, A., 2006. Preferential erosion of black carbon on steep slopes with slash and burn agriculture. *Catena* 65, 30–40. doi:10.1016/j.catena.2005.09.005
- 830 Rumpel, C., Leifeld, J., Santin, C., Doerr, S., 2015. Movement of biochar in the environment, in: Lehmann, J., Joseph, S. (Eds.), *Biochar for Environmental Management*. Routledge, pp. 281–298.
- Saiz, G., Goodrick, I., Wurster, C., Nelson, P.N., Wynn, J., Bird, M., 2018. Preferential Production and Transport of Grass-Derived Pyrogenic Carbon in NE-Australian Savanna Ecosystems. *Frontiers in Earth Science* 5, 1–13.



- 835      doi:10.3389/feart.2017.00115
- Santín, C., Doerr, S.H., Kane, E.S., Masiello, C.A., Ohlson, M., de la Rosa, J.M., Preston, C.M., Dittmar, T., 2016. Towards a global assessment of pyrogenic carbon from vegetation fires. *Global Change Biology* 22, 76–91.  
doi:10.1111/gcb.12985
- Santín, C., Doerr, S.H., Preston, C.M., González-Rodríguez, G., 2015. Pyrogenic organic matter production from wildfires: a  
840      missing sink in the global carbon cycle. *Global Change Biology* 21, 1621–1633. doi:10.1111/gcb.12800
- Schindler Wildhaber, Y., Bänninger, D., Burri, K., Alewell, C., 2012. Evaluation and application of a portable rainfall simulator on subalpine grassland. *Catena* 91, 56–62. doi:10.1016/j.catena.2011.03.004
- Shakesby, R.A., 2011. Post-wildfire soil erosion in the Mediterranean: Review and future research directions. *Earth-Science Reviews* 105, 71–100. doi:10.1016/j.earscirev.2011.01.001
- 845      Shakesby, R.A., Bento, C.P.M., Ferreira, C.S.S., Ferreira, A.J.D., Stoof, C.R., Urbanek, E., Walsh, R.P.D., 2015. Impacts of prescribed fire on soil loss and soil quality: An assessment based on an experimentally-burned catchment in central Portugal. *Catena* 128, 278–293. doi:10.1016/j.catena.2013.03.012
- Shakesby, R.A., Doerr, S.H., 2006. Wildfire as a hydrological and geomorphological agent. *Earth-Science Reviews* 74, 269–307. doi:10.1016/j.earscirev.2005.10.006
- 850      Singh, N., Abiven, S., Maestrini, B., Bird, J.A., Torn, M.S., Schmidt, M.W.I., 2014. Transformation and stabilization of pyrogenic organic matter in a temperate forest field experiment. *Global Change Biology* 20, 1629–1642. doi:10.1111/gcb.12459
- Singh, N., Abiven, S., Torn, M.S., Schmidt, M.W.I., 2012. Fire-derived organic carbon in soil turns over on a centennial scale. *Biogeosciences* 9, 2847–2857. doi:10.5194/bg-9-2847-2012
- 855      Soucémarianadin, L., Reisser, M., Cécillon, L., Barré, P., Nicolas, M., Abiven, S., 2019. Pyrogenic carbon content and dynamics in top and subsoil of French forests. *Soil Biology and Biochemistry* 133, 12–15. doi:10.1016/j.soilbio.2019.02.013
- Spokas, K.A., Novak, J.M., Masiello, C.A., Johnson, M.G., Colosky, E.C., Ippolito, J.A., Trigo, C., 2014. Physical Disintegration of Biochar: An Overlooked Process. *Environmental Science and Technology Letters* 1, 326–332.  
860      doi:10.1021/ez500199t
- Stallard, R.F., 1998. Terrestrial sedimentation and the carbon cycle: Coupling weathering and erosion to carbon burial. *Global Biogeochemical Cycles* 12, 231–257. doi:10.1029/98GB00741
- Stoof, C.R., Gevaert, A.I., Baver, C., Hassanpour, B., Morales, V.L., Zhang, W., Martin, D., Giri, S.K., Steenhuis, T.S., 2016. Can pore-clogging by ash explain post-fire runoff? *International Journal of Wildland Fire* 25, 294–305.  
865      doi:10.1071/WF15037
- Thomaz, E.L., 2018. Interaction between ash and soil microaggregates reduces runoff and soil loss. *Science of the Total Environment* 625, 1257–1263. doi:10.1016/j.scitotenv.2018.01.046
- Tinner, W., Hofstetter, S., Zeugin, F., Conedera, M., Wohlgemuth, T., Zimmermann, L., Zweifel, R., 2006. Long-distance



- 870 transport of macroscopic charcoal by an intensive crown fire in the Swiss Alps - implications for fire history  
reconstruction. *The Holocene* 16, 287–292.
- van der Werf, G.R., Randerson, J.T., Giglio, L., Leeuwen, T.T. Van, Chen, Y., Collatz, G.J., Yokelson, R.J., Kasibhatla,  
P.S., 2017. Global fire emissions estimates during 1997 – 2016. *Earth System Science Data* 9, 697–720.
- Vieira, D.C.S., Fernández, C., Vega, J.A., Keizer, J.J., 2015. Does soil burn severity affect the post-fire runoff and interrill  
erosion response? A review based on meta-analysis of field rainfall simulation data. *Journal of Hydrology* 523, 452–  
875 464. doi:10.1016/j.jhydrol.2015.01.071
- Vieira, D.C.S., Malvar, M.C., Martins, M.A.S., Serpa, D., Keizer, J.J., 2018. Key factors controlling the post-fire  
hydrological and erosive response at micro-plot scale in a recently burned Mediterranean forest. *Geomorphology* 319,  
161–173. doi:10.1016/j.geomorph.2018.07.014
- Wang, Z., Govers, G., Steegen, A., Clymans, W., Van den Putte, A., Langhans, C., Merckx, R., Van Oost, K., 2010.  
880 Catchment-scale carbon redistribution and delivery by water erosion in an intensively cultivated area. *Geomorphology*  
124, 65–74. doi:10.1016/j.geomorph.2010.08.010
- Westerling, A.L., Hidalgo, H.G., Cayan, D.R., Swetnam, T.W., 2006. Warming and earlier spring increase Western U.S.  
forest wildfire activity. *Science* 313, 940–943. doi:10.1126/science.1128834



885 **Table 1: Total organic carbon (TOC), soil organic carbon stock (SOC),  $\delta^{13}\text{C}$ , bulk density, soil texture, pH, aggregate stability (mean weight diameter (MWD)), runoff ratio (runoff/rainfall) and soil water repellency of the Cambisol and Luvisol. Average values  $\pm$  1 standard error.**

	Cambisol		haplic Luvisol	
TOC [%]	3.6 $\pm$ 0.4 (n = 72)		2.24 $\pm$ 0.02 (n = 72)	
SOC stock [Mg / ha] <sup>1</sup>	36.0 $\pm$ 4.0 (n = 72)		23.4 $\pm$ 0.2 (n = 72)	
$\delta^{13}\text{C}$ [‰]	-29.07 $\pm$ 0.05 (n = 72)		-29.87 $\pm$ 0.03 (n = 72)	
<b>Bulk density</b> [g/cm <sup>3</sup> ]	Before rainfall 0.94 $\pm$ 0.03 (n = 4)	After rainfall 1.01 $\pm$ 0.03 (n = 4)	Before rainfall 0.97 $\pm$ 0.01 (n = 4)	After rainfall 1.11 $\pm$ 0.03 (n = 4)
<b>Texture</b> [%]	Clay loam <sup>2</sup> Sand: 45.5 $\pm$ 3.5 Silt: 24.2 $\pm$ 4.4 Clay: 31.5 $\pm$ 2.4		Sandy silt <sup>3</sup> Sand: 40 Silt: 40 Clay: 20	
<b>pH [-]</b>	5.9 $\pm$ 0.5 <sup>2</sup>		3.9 <sup>3</sup>	
<b>Aggregate stability</b> [MWD]	1.74 $\pm$ 0.03 (n = 6)		0.89 $\pm$ 0.03 (n = 6)	
<b>Runoff ratio [%]<sup>4</sup></b> [Runoff (l) /rainfall (mm)]	13.2 $\pm$ 0.8 (n = 32) (1.7 $\pm$ 0.1 / 51.4 $\pm$ 1.4)		88.5 $\pm$ 2.3 (n = 32) (11.4 $\pm$ 0.3 / 51.4 $\pm$ 1.4)	
<b>Water repellency<sup>5</sup></b>	Very hydrophilic to hydrophilic (n = 5)		Very hydrophilic (n = 5)	

<sup>1</sup>Calculated after M4 in Poeplau et al. (2017). <sup>2</sup>Maestrini et al. (2014). <sup>3</sup>Braun et al. (2020). <sup>4</sup>Recorded runoff (l) was converted to runoff (m<sup>3</sup>). Runoff (m<sup>3</sup>) was divided by the soil plot area (0.25 m<sup>2</sup>) to calculate runoff depth (m). The runoff depth (mm) was then divided by the rainfall depth (mm) to calculate the runoff ratio (%). <sup>5</sup>According to the classification by Doerr (1998).

890

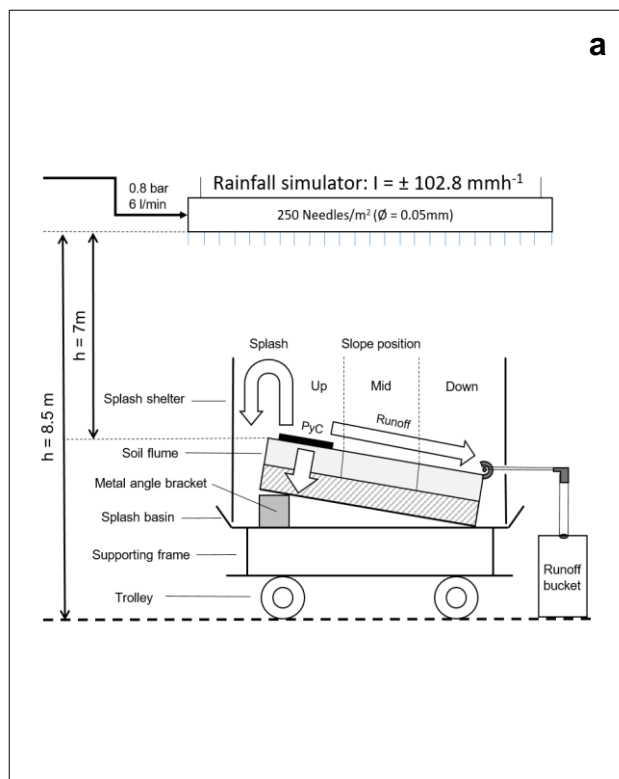
**Table 2: Total C,  $\delta^{13}\text{C}$  and water repellency of wood-PyC (derived from *Picea abies*) and grass-PyC (derived from *Miscanthus sinensis*). Average values  $\pm$  1 standard error.**

	Wood-PyC ( <i>Picea abies</i> )	Grass-PyC ( <i>Miscanthus sinensis</i> )
<b>Total C [%]</b>	64.9 $\pm$ 1.3 (n = 5)	68.6 $\pm$ 1.8 (n = 5)
$\delta^{13}\text{C}$ [‰]	-38.2 $\pm$ 0.2 (n = 5)	-13.8 $\pm$ 0.1 (n = 5)
<b>Water repellency<sup>1</sup></b>	Extremely hydrophobic (n = 5)	Extremely hydrophobic (n = 5)

<sup>1</sup>According to classification by Doerr (1998).



## Experimental setup



## PyC surface dynamics

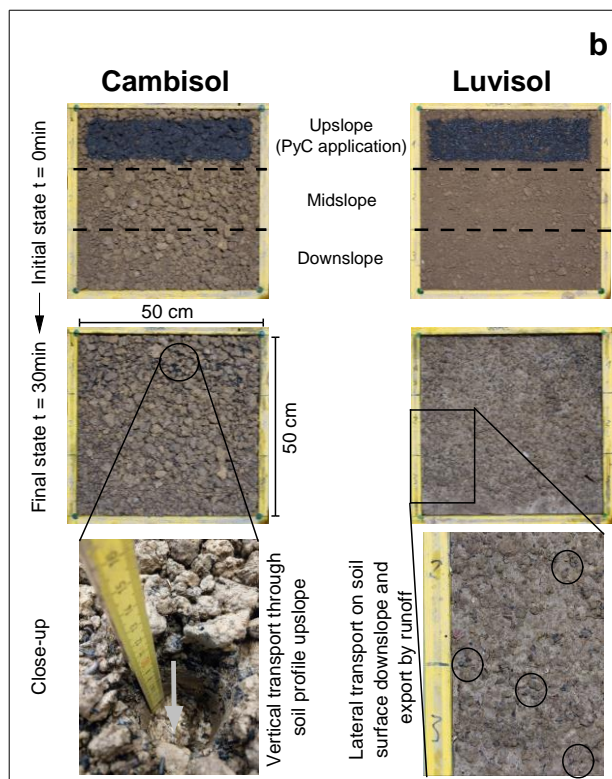


**Figure 1: Experimental setup, including the rainfall simulator and an example of a 0.25-m<sup>2</sup> soil plot (a) and visual assessment of the surface of the Cambisol and Luvisol (25° slope and with coarse wood-PyC) (b). Each 0.25-m<sup>2</sup> soil plot was photographed before and after the 30 minutes rainfall simulation experiment. Visual assessment showed vertical movement of PyC in the Cambisol (white arrow in Fig. 1b) and surface redistribution of PyC on the Luvisol (black circles in Fig. 1b).**



895

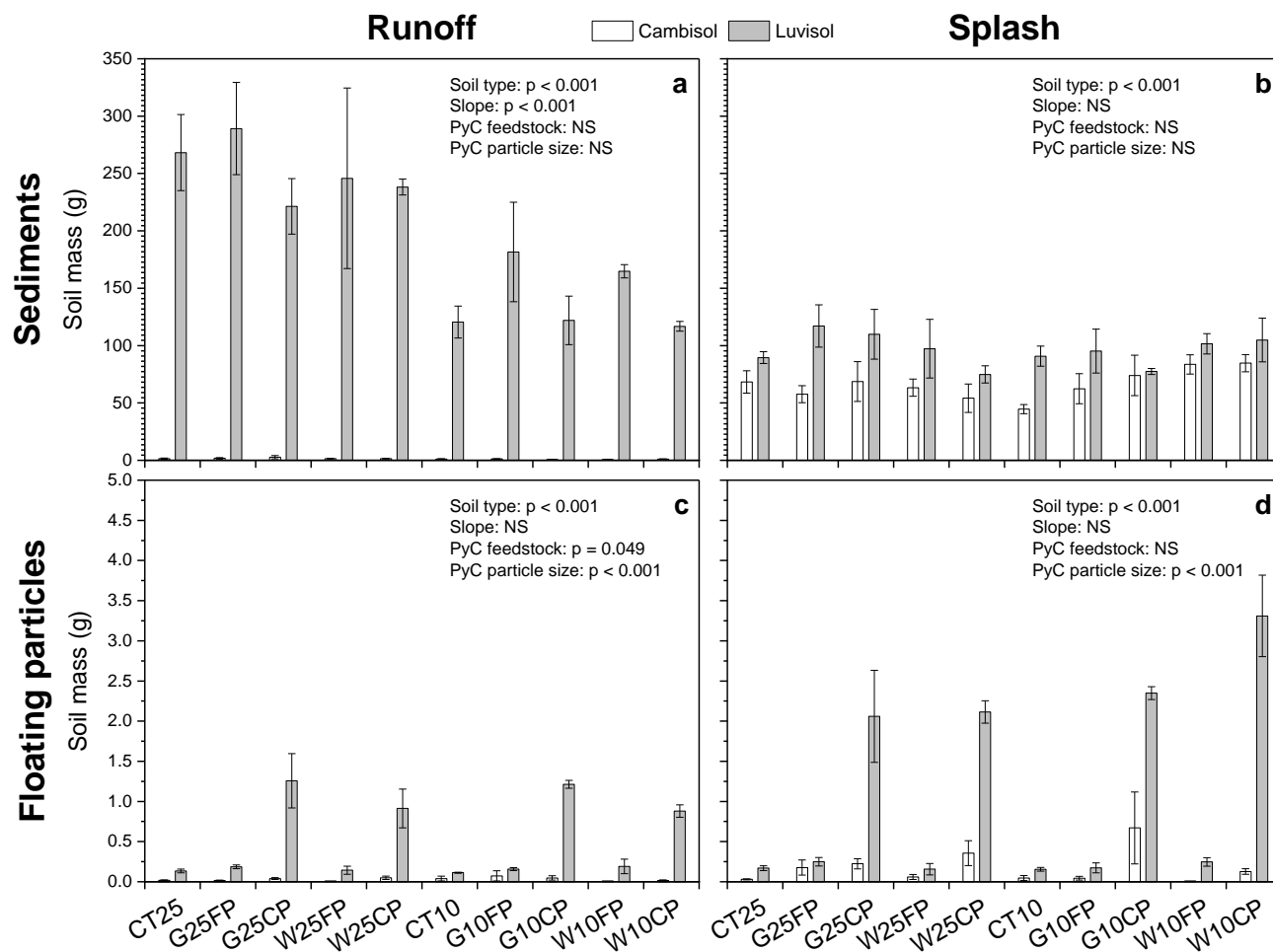


**Figure 2: Amount of sediment [in g] transported by the runoff (a) and splash (b), as well as floating particles transported by runoff (c) and splash (d) for each treatment after 30 minutes of rainfall (total:  $51.4 \pm 1.4$  mm) (CT = control plots; G = grass-PyC; W = wood-PyC; 25 =  $25^\circ$  slope; 10 =  $10^\circ$  slope; FP = fine PyC ( $< 63 \mu\text{m}$ ); CP = coarse PyC ( $63 \mu\text{m}$  to  $2 \text{mm}$ )). Values are given as means ( $\pm 1$  standard error) and correspond to the mass of soil for control plots (CT:  $n = 4$ ) and mass of soil + PyC for plots where PyC was applied ( $n = 3$ ; PyC only represented  $< 2\%$  of total mass).**

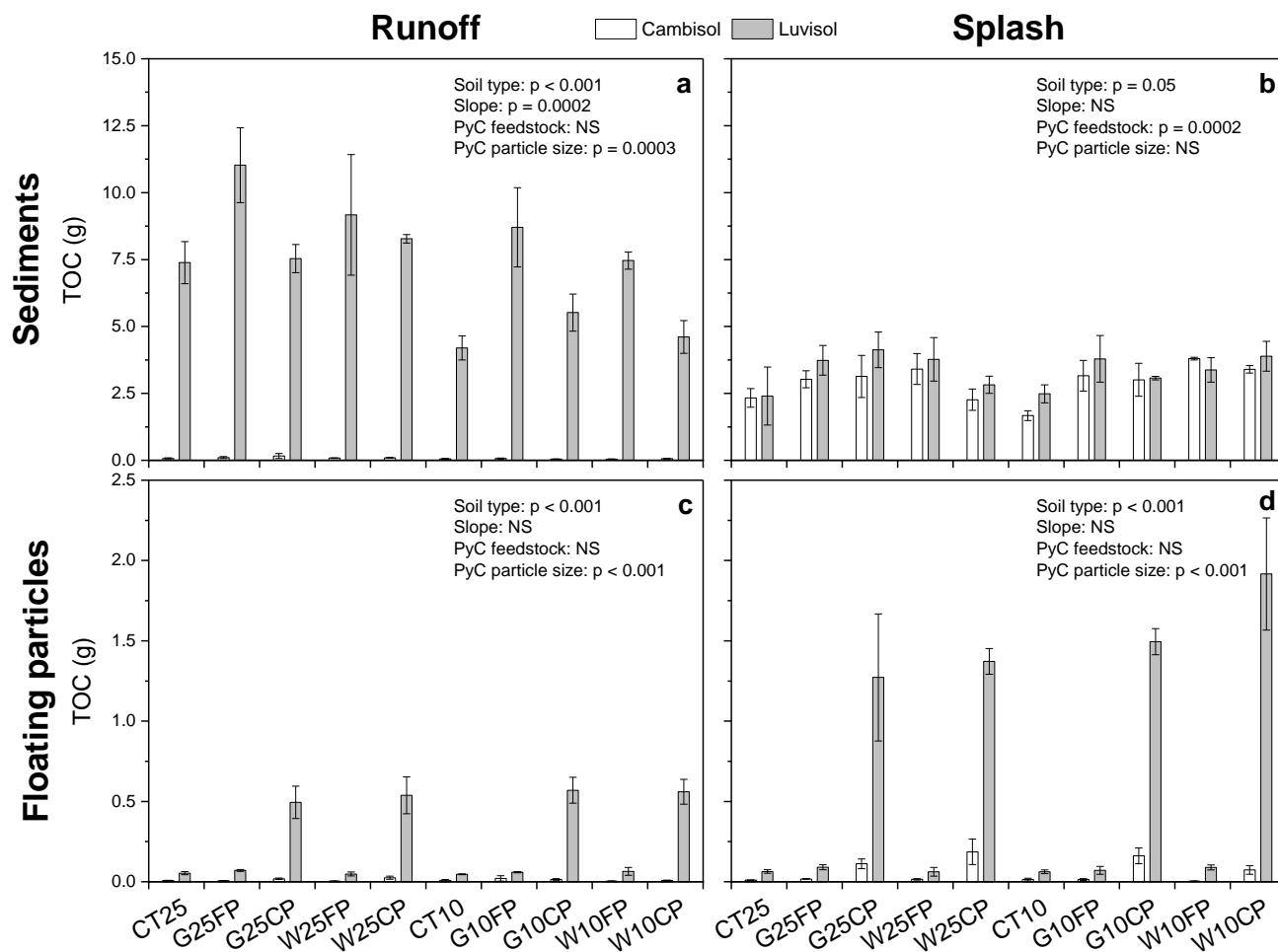


**Figure 3:** Amount of TOC [in g] transported by runoff (a) and splash sediment (b), as well as the floating particles in runoff (c) and splash (d) for each treatment after 30 minutes of rainfall (total:  $51.4 \pm 1.4$  mm) (CT = control plots; G = grass-PyC; W = wood-PyC; 25 =  $25^\circ$  slope; 10 =  $10^\circ$  slope; FP = fine PyC ( $< 63 \mu\text{m}$ ); CP = coarse PyC ( $63 \mu\text{m}$  to  $2 \text{mm}$ )). Values are given as means ( $\pm 1$  standard error) and the TOC values represent native SOC (nSOC) for control plots (CT:  $n = 4$ ) and nSOC + PyC for plots where PyC was applied ( $n = 3$ ).

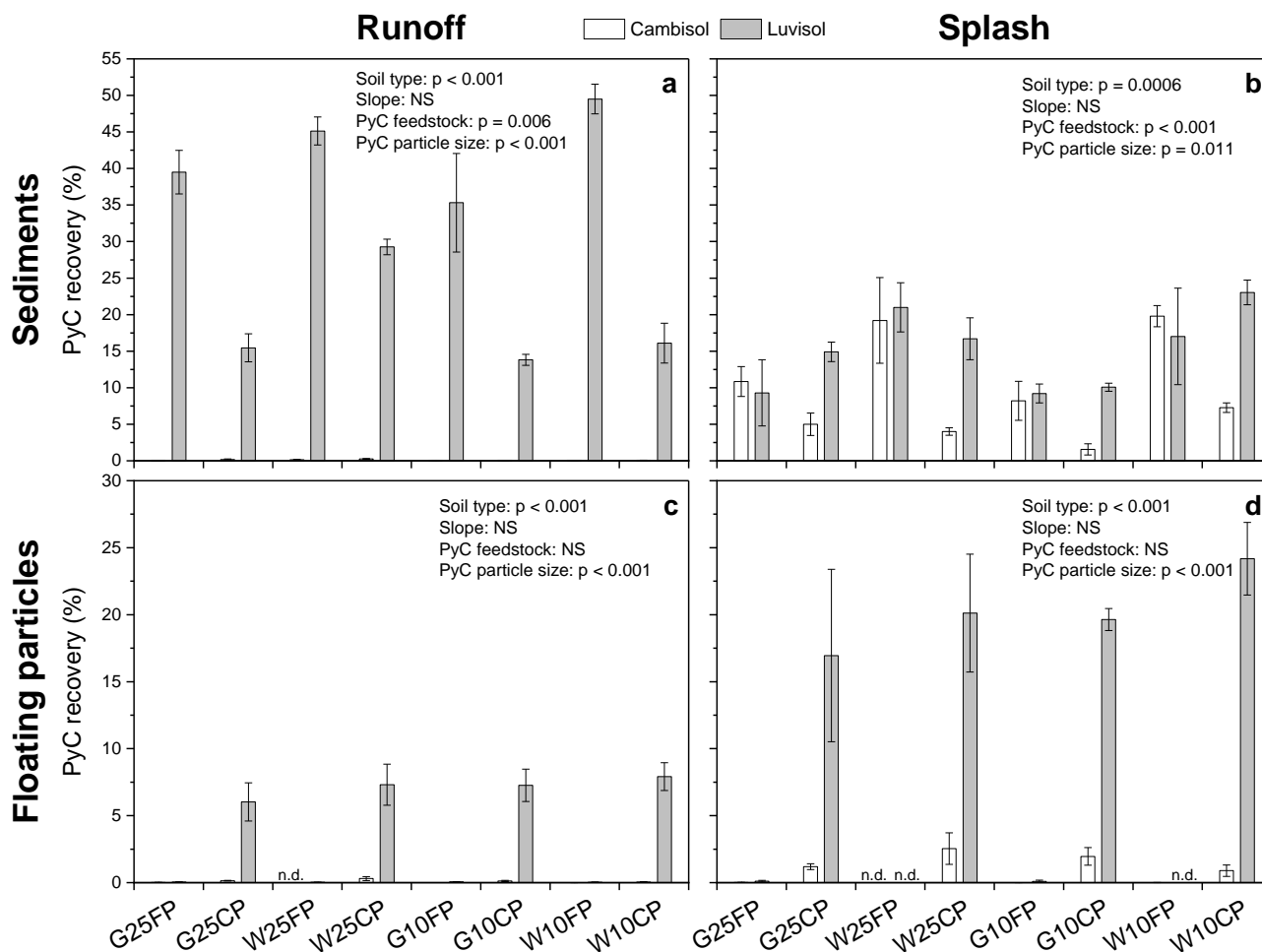


**Figure 4:** PyC recovery [% of total added PyC] in sediment transported by runoff (a) or splash (b), and floating particles transported by runoff (c) and splash (d) for each treatment after 30 minutes of rainfall (total:  $51.4 \pm 1.4$  mm) (G = grass-PyC; W = wood-PyC; 25 = 25° slope; 10 = 10° slope; FP = fine PyC (< 63  $\mu$ m); CP = coarse PyC (63  $\mu$ m to 2 mm)). Average values  $\pm 1$  standard error (n = 3).

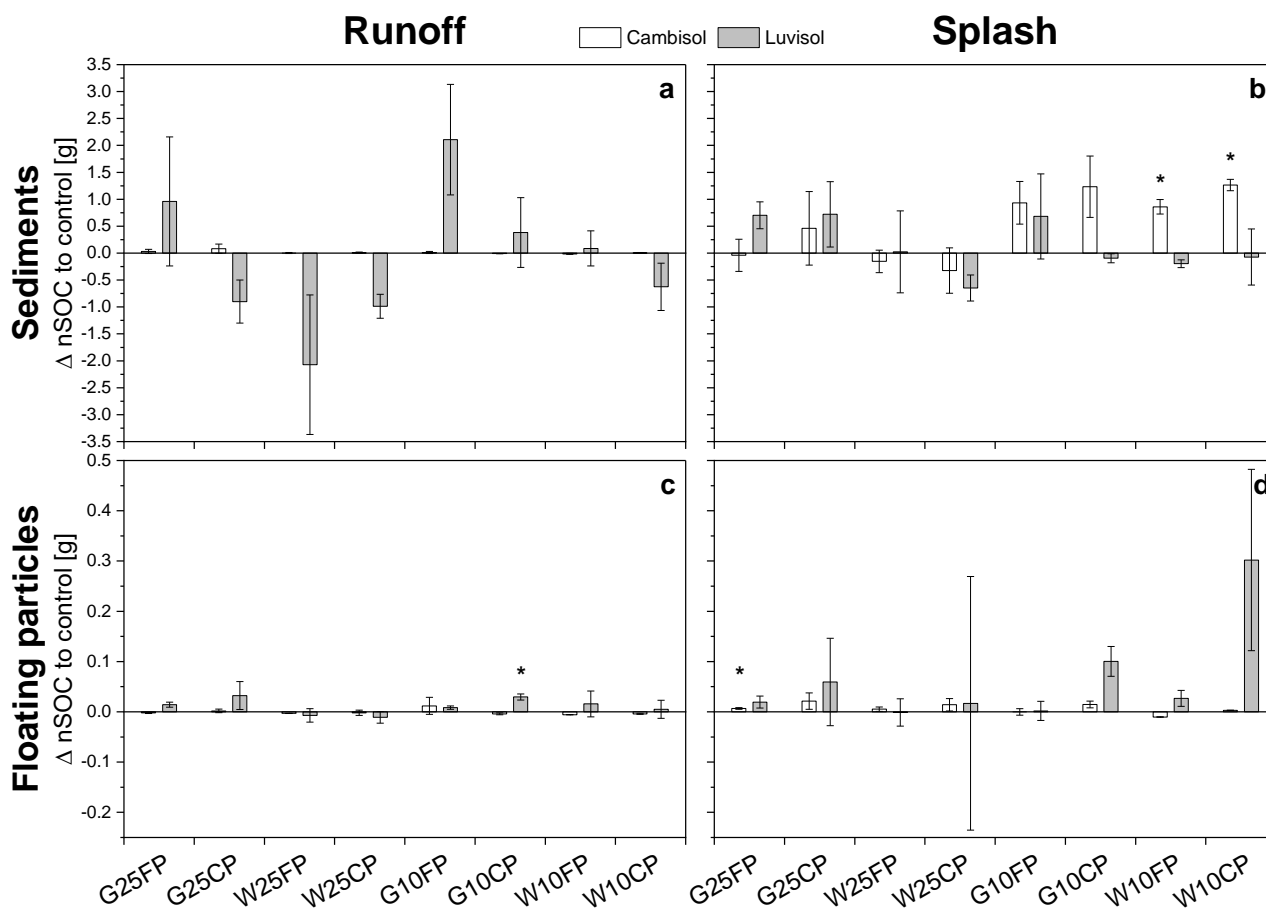


**Figure 5: Differences in native SOC export [ $\Delta$  nSOC to control in g] between the PyC treatments (nSOC = TOC – PyC) and the corresponding controls (nSOC = TOC) in sediment transported by runoff (a), splash (b), as well as floating particles in runoff (c) and splash (d) after 30 minutes of rainfall (total  $51.4 \pm 1.4$  mm) (G = grass-PyC; W = wood-PyC; 25 =  $25^\circ$  slope; 10 =  $10^\circ$  slope; FP = fine PyC (<  $63 \mu\text{m}$ ); CP = coarse PyC ( $63 \mu\text{m}$  to  $2 \text{mm}$ )). Average values  $\pm$  1 standard error (n = 3). Significant changes at  $p < 0.05$  are marked with an asterisk (\*).**

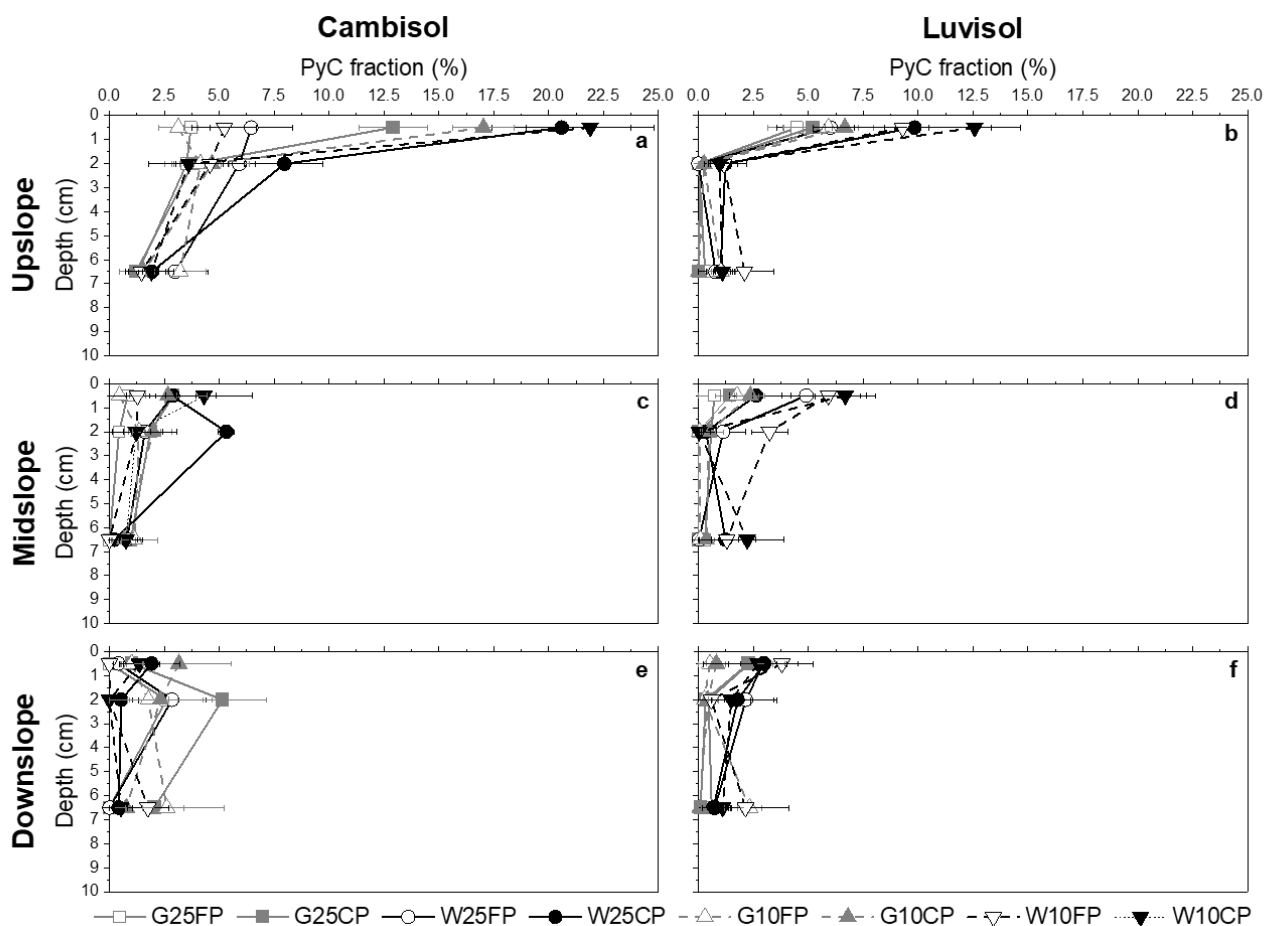


**Figure 6:** Distribution of PyC [PyC fraction = fraction of OC derived from the PyC in %] in soil cores for the Cambisol (a, c and e) and Luvisol (b, d and f) along the 0.25-m<sup>2</sup> plot (Upslope: a-b; midslope: c-d and downslope: e-f) and with depth (0-1, 1-3, 3-10 cm) for each treatment after 30 minutes rainfall (total: 51.4 ± 1.4 mm) (G = grass-PyC; W = wood-PyC; 25 = 25° slope; 10 = 10° slope; FP = fine PyC (< 63 μm); CP = coarse PyC (63 μm to 2 mm)). Average values ± 1 standard error (n = 3).